ANL-78-45

HIGH-PERFORMANCE BATTERIES FOR STATIONARY ENERGY STORAGE AND ELECTRIC-VEHICLE PROPULSION

Progress Report for the Period January—March 1978

U of C-AUA-USDOE

ARGONNE NATIONAL LABORATORY, ARGONNE, ILLINOIS

Prepared for the U. S. DEPARTMENT OF ENERGY
under Contract W-31-109-Eng-38

Printed in the United States of America
Available from
National Technical Information Service
U. S. Department of Commerce
5285 Port Royal Road
Springfield, Virginia 22161
Price: Printed Copy $6.00; Microfiche $3.00

Distribution Category:
Energy Storage—Electrochemical—
Advanced Batteries (UC-94cb)

ANL-78-45

ARGONNE NATIONAL LABORATORY
9700 South Cass Avenue
Argonne, Illinois 60439

HIGH-PERFORMANCE BATTERIES FOR STATIONARY ENERGY STORAGE AND ELECTRIC-VEHICLE PROPULSION

Progress Report for the Period
January—March 1978

P. A. Nelson	Director, Energy Storage
R. K. Steunenberg	Manager, Lithium/Metal Sulfide Battery Program
A. A. Chilenskas	Manager, Battery Commercialization
E. C. Gay	Section Manager, Battery Engineering
J. E. Battles	Group Leader, Materials Development
F. Hornstra	Group Leader, Battery Charging Systems
W. E. Miller	Group Leader, Industrial Cell and Battery Testing
M. F. Roche	Group Leader, Cell Chemistry
H. Shimotake	Group Leader, Cell Development and Engineering

July 1978

Previous Reports in this Series

ANL-77-35	January—March 1977
ANL-77-68	April—June 1977
ANL-77-75	July—September 1977
ANL-78-21	October—December 1977

PREFACE

The program on high-temperature secondary batteries at Argonne National Laboratory consists of an in-house research and development effort and subcontracted work by industrial laboratories. The work at Argonne is carried out primarily in the Chemical Engineering Division, with assistance on specific problems being given by the Materials Science Division and, from time to time, by other Argonne divisions. The individual efforts of many scientists, engineers, and technicians are essential to the success of the program, and recognition of these efforts is reflected by the individual contributions cited throughout the report.

TABLE OF CONTENTS

	Page
ABSTRACT	1
SUMMARY	2
I. INTRODUCTION	7
II. COMMERCIAL DEVELOPMENT	9
A. Commercialization Studies	9
B. Systems Design	10
1. Design Studies for a Stationary Energy Storage Module	10
2. Design Studies for Electric-Vehicle Batteries	11
III. INDUSTRIAL CELL AND BATTERY TESTING	18
A. Testing of Contractor Produced Cells	18
1. Qualification Testing of Eagle-Picher Cells	18
2. Other Tests on Eagle-Picher Cells	21
3. Qualification Testing of Gould Cells	24
4. Lifetime Testing of Gould Cells	26
5. Tests on Atomics International's Cells	26
B. The Mark IA Battery	27
C. Equipment for Cell and Battery Tests	28
1. Stationary Testing Facilities for Batteries	28
2. Lifetime Test Facility for up to 100 Cells	29
3. Equipment for Testing Batteries in Vehicles	29
IV. CELL DEVELOPMENT AND ENGINEERING	33
A. Development of FeS Cells	33
1. Uncharged Cells with Pressed Electrodes	33
2. Charged FeS Cells with Pressed Electrodes	34
3. Small-Scale FeS Cells	35
4. Multiplate Cell Design	35
B. Development of MS_2 Cells	36
1. Uncharged MS_2 Cells with Pressed Electrodes	37
2. Charged MS_2 Cells with Pressed Electrodes	37
3. Carbon-Bonded MS_2 Cells	39
V. MATERIALS DEVELOPMENT	42
A. Electrode Separator Development	42
1. In-Cell Testing	42
2. Out-of-Cell Testing	42
B. Ceramic Materials Development	43

TABLE OF CONTENTS (contd)

		Page
C.	Cell Wetting and Degassing Studies	46
D.	Corrosion Studies	47
E.	Post-Test Cell Examinations	48
1.	Causes of Cell Failure	49
2.	In-Cell Corrosion Results	53
VI.	CELL CHEMISTRY	55
A.	Chemical Conditions for the Formation of J Phase	55
B.	Effects of Electrolyte Composition and Cell Temperature on FeS Cell Performance	56
VII.	ADVANCED BATTERY RESEARCH	58
A.	Engineering-Scale Cell Tests	58
B.	Cell Development	59
1.	Positive Electrode Development	59
2.	Negative Electrode Development	60
3.	Electrolyte Development	61
REFERENCES		63
APPENDIX A		64

LIST OF FIGURES

No.	Title	Page
II-1.	Battery Jacket Design	13
III-1.	The Specific Energy of Cell I-8-L-034	20
III-2.	The Specific Power of Cell I-8-L-034	20
III-3.	Effect of Cell Temperature on Capacity of Cell I-3-C-2	22
III-4.	Open Circuit Voltage *vs.* State of Discharge for Cell I-3-C-1	23
III-5.	Voltage *vs.* Capacity Curve for Cell GO4-010	26
III-6.	Block Diagram of Data Acquisition and Processing Systems for In-Vehicle Battery Performance Evaluation	31
IV-1.	Utilization of Three R-Series Cells	34
IV-2.	Multiplate Cell Design	36
IV-3.	Performance Data on Cell M-4	38
IV-4.	Performance Data on Cell PW-9	41
V-1.	Creep Behavior of FeS + LiCl-KCl Sample at 450°C	43
V-2.	Microstructure of a Y_2O_3 Sample Prepared from Crushed Y_2O_3-Nitric Acid Plaster	45
V-3.	Corrosion of Low-Carbon-Steel Current Collector by the Negative Electrode	54
V-4.	Corrosion of Molybdenum Current Collector in the Positive Electrode	54
VII-1.	Performance of $Ca(Mg_2Si)$/NiS Cell	59

LIST OF TABLES

No.	Title	Page
I-1.	Technical Goals for the Mark IA Battery	8
II-1.	World and United States Reserves of B_2O_3 and Ores in 1978	9
II-2.	Projected Boron Demand in the United States	10
II-3.	Estimated Heat Loss from Various Battery Jackets	14
II-4.	Assumptions for Thermal Analysis of a 50 kW-hr Battery	16
II-5.	Driving Cycle No. 1	16
II-6.	Driving Cycle No. 2	17
III-1.	Capacity of Four FeS Cells at Various Operating Temperatures	21
III-2.	Performance Data on 15 Gould FeS_2 Cells	25
III-3.	Operation Criteria for Mark IA Battery	27
IV-1.	Materials Costs for the ANL Multiplate Cell	37
IV-2.	Performance Data on Cells M-4 and M-7	38
IV-3.	Resistances of KK-series Cells	39
V-1.	Density Data for Various Sintered Y_2O_3 Specimens	45
V-2.	Corrosion Rates for Selected Metals Tested at 450°C in Equal Volume Mixtures of Metal Sulfides and Electrolyte	48
V-3.	Results of Post-test Cell Examinations	50
V-4.	Causes of Cell Failure	53
VI-1.	Maximum Temperature for Formation of J Phase in FeS Electrodes	56
VI-2.	Utilization of Positive Electrode in LiAl/LiCl-KCl/FeS Cells	57
VII-1.	Melting Points of Electrolytes	61

HIGH-PERFORMANCE BATTERIES FOR STATIONARY ENERGY STORAGE AND ELECTRIC-VEHICLE PROPULSION

Progress Report for the Period
January—March 1978

ABSTRACT

This report covers the research, development, and management activities of the program at Argonne National Laboratory (ANL) on lithium/metal sulfide batteries during January-March 1978. These batteries are being developed for electric-vehicle propulsion and for stationary energy storage applications. The present cells, which operate at 400-500°C, are of a vertically oriented, prismatic design with one or more positive electrodes of metal sulfide (usually, FeS or FeS_2), faced on both sides by negative electrodes of lithium-aluminum or lithium-silicon alloy. The electrolyte is molten LiCl-KCl eutectic (m.p., 352°C). An important advance in cell design has been the successful development of multiple-electrode cells, which have higher specific energy and specific power than the earlier bicell (one positive electrode) designs.

A major objective of this program is to transfer the technology to industry as it is developed, with the ultimate goal of a competitive, self-sustaining industry for the commercial production of lithium/metal sulfide batteries. Technology transfer is implemented by several means, including the assignment of industrial participants to ANL for various periods of time and the subcontracting of development and fabrication work on cells, batteries, and auxiliary items to industrial firms.

Under a subcontract with ANL, cell fabrication is done at Atomics International Division of Rockwell International, Eagle-Picher Industries, Inc., and Gould Inc. Testing and evaluation of cells fabricated by these firms are performed at the subcontractor's facilities or at ANL. The most significant event during this period was the initiation of an effort to design, develop, and fabricate a 40-kW-hr electric-vehicle battery (Mark IA) by Eagle-Picher Industries. The Mark IA is scheduled for testing in a van early in 1979.

Conceptual design studies of a 100 MW-hr energy-storage plant have been under way both at ANL and Atomics International. These two conceptual designs are currently being merged into one.

In-house efforts at ANL have continued on cell and battery development, materials development and evaluation, cell-chemistry investigations, battery design and commercialization studies, and the development of advanced, high-temperature batteries that use inexpensive, abundant materials.

SUMMARY

Battery Design and Commercial Development

An estimate of the manufacturing cost for Li-Al/MS_x cells was presented in ANL-76-12 (March 1976). This study is being updated. In other commercialization studies, the impact of large-scale production of lithium/metal sulfide batteries on boron reserves in the U. S., as well as the world, was examined. The results show that U. S. reserves are adequate for approximately 85 years and that world boron resources are adequate for hundreds of years.

Conceptual design studies of batteries for electric-vehicle and stationary storage applications are under way. A cooperative effort between the Atomic International Division of Rockwell International and ANL is in progress to develop a conceptual design of a 5.6-MW truckable battery for stationary energy studies. This design will use either lithium-silicon or lithium-aluminum/FeS cells.

The effort on electric-vehicle battery design was focused on thermal management of these batteries. A conceptual design of a battery jacket consisting of vacuum-foil insulation and structural supports was developed, and the feasibility of using this design in the Mark IA battery (40 kW-hr) was assessed.

Calculations were made of the heat generated by a cell during operation; this information will be used in the design of a heating/cooling system for a 40 kW-hr battery (Mark IA). An analysis was performed to determine the cost of maintaining the required operating temperature of a 50 kW-hr battery (Mark II) in an electric vehicle that is driven 16000 km/yr. No heating or cooling of the battery during driving was assumed. The results indicated that the cost required to maintain the battery temperature at the required level is minimal.

In other electric-vehicle battery design work, a conceptual design for a battery charger (designed by TRW, Inc.) has been selected. This charger will use the shunt-current interrupt technique to achieve cell equalization, and a current-interrupt technique to monitor cell voltage.

Industrial Cell and Battery Testing

Eagle-Picher Industries, Inc. fabricated a group of Li-Al/FeS_2 cells with a design similar to that of their Type I-7 cell, which had the most compact design and highest performance of any cell produced by Eagle-Picher up to that time. Some of the Type I-8 cells had molybdenum-screen particle retainers, others had no particle retainers. After the Type I-8 cells were filled with electrolyte, their resistance at room temperature ("frozen" resistance) ranged from 0.1 to 3×10^6 Ω. Attempts to cycle those cells with low frozen resistances led to early cell failure. Investigations by Eagle-Picher led to the conclusion that active material from the electrodes had escaped during the electrolyte filling operation. Appropriate corrective actions (the use of molybdenum screens and Y_2O_3-felt particle retainers and the elimination of fine particle size active material) in replacement cells eliminated this problem. These replacement cells will be used to conduct tests on the effect of extensive vibrations on these cells.

One of the defective Type I-8 cells with a frozen resistance of 3×10^6 Ω was tested at ANL. This cell, although it short-circuited within 20 cycles, had the best performance of any Eagle-Picher cell produced to date (specific energy, 90 W-hr/kg at the 4-hr rate; peak specific power, 65 W/kg).

Tests were conducted at ANL on Eagle-Picher LiAl/FeS-Cu_2S cells to determine the effect on performance of (1) the use of a LiCl-rich electrolyte, *i.e.*, 67 mol % LiCl-33 mol % KCl and (2) operation at a high temperature (∿500°C). The results indicated that the use of LiCl-rich electrolyte in a LiAl/FeS-Cu_2S cell does not improve performance over that of a similar cell with eutectic electrolyte, but that operation at 500°C improves cell capacity over that at 425°C. In the latter case, the high-temperature operation resulted in a lowering of the coulombic efficiency in two of the four cells undergoing thermal tests.

Gould Inc. is fabricating 55 upper-plateau FeS_2 cells under a subcontract from ANL. These cells are being tested to determine the effect on performance of current collector design, lithium content of the negative electrode, electrolyte volume and thickness of the positive electrode, and method of particle retention. To date, 15 Gould cells have been qualification tested. This testing indicated that the capacity of some of these cells was limited by the negative electrode. Nevertheless, high utilization of the upper plateau was achieved in these cells. Cell G-04-010, for instance, had a utilization of 85% and a specific energy of 75 W-hr/kg at a current density of 100 mA/cm^2.

Eagle-Picher Industries has been awarded the Mark IA battery contract. This contract entails the development, design and fabrication of a 40 kW-hr battery by early 1979. This battery will undergo stationary and in-vehicle testing at ANL.

A facility for testing up to 100 industrial cells is currently being constructed at ANL; to be included as an integral part of this facility is a computer system for monitoring of cell performance and data acquisition. This facility will be used primarily for lifetime testing of industrial cells. A facility is also being constructed for laboratory tests of large-scale (up to 60 kW-hr) batteries that will precede in-vehicle tests. This facility will have the capability for computer-controlled operation and data acquisition. In addition, equipment for in-vehicle testing of batteries is being designed.

Cell Development and Engineering

Cell development work is being conducted to improve the performance of Li-Al/MS_x cells.

During this reporting period, an attempt was made to improve the performance of the FeS cell by either of two methods--the use of a LiCl-rich electrolyte (61 mol % LiCl-39 mol % KCl) or the addition of 16 mol % Cu_2S to the positive electrode. Cell tests indicated that both of these methods improve electrode utilization by 10-20%. Therefore, an M-series cell (these cells are designed as compactly as state-of-the-art technology permits) was constructed with 16 mol % Cu_2S added to the positive electrode and eutectic electrolyte, and another M-series cell was constructed with no copper additive and LiCl-rich electrolyte. Cell testing showed that the specific energies and resistances of these two cells were similar (54-56 W-hr/kg at a current density of 74 mA/cm^2 and 3.5-5.0 mΩ).

In order to further increase the specific energy of the Li-Al/FeS cell, the use of multiplate cells has been proposed. This cell design consists of three negative electrodes of Li-Al alloy, two positive electrodes of metal sulfide, a BN-felt separator, and a molten LiCl-KCl electrolyte. Calculations indicate that the multiplate FeS cell should achieve a specific energy of 131 W-hr/kg at the 4-hr rate.

Investigations are continuing on Li-Al/FeS_2 cells in which part or all of the iron sulfide in the positive electrode is replaced by nickel sulfide. In general, the cells with nickel sulfide in the positive electrode have shown better capacity retention and longer lifetimes than cells with FeS_2 positive electrodes.

A review of the cells with carbon-bonded FeS_2 electrodes showed that cell resistance is strongly affected by the current-collector design. The cells with the lowest resistance (3.5-5.5 mΩ) had a vertical terminal rod of molybdenum that extended into the active material and was welded to the molybdenum current collector.

Three Li-Al/FeS cells with MgO powder separators, PW-8, -9, and -10, have maintained stable operation for over 171, 65, and 63 days, respectively.

Materials Development

Operation of a Li-Al/FeS separator-test cell, which had a separator of 1.25-mm-thick BN felt, was terminated after 71 days (98 cycles). This test cell had a specific energy of 66 W-hr/kg at a discharge current density of 40 mA/cm^2. Out-of-cell testing is also being done to characterize BN felts fabricated by the Carborundum Co.

Flowability studies were conducted to determine the stress levels required to initiate flow (creep) in FeS electrodes. Significant flow of FeS-electrolyte mixtures occurred at stress levels of 210-240 kPa (30-35 psi). This behavior is consistent with the observed tendency of inadequately constrained positive electrodes to extrude out of the electrode.

Efforts have continued on the development of sintered, porous ceramic separators. Results have shown that separator plates of suitable dimensions for in cell-testing, high porosities, and good strength can be obtained by cold pressing and sintering of as-received Y_2O_3, crushed Y_2O_3 plaster, and calcined Y_2O_3 plaster. The separators made from these materials will be submitted to in-cell testing during the next quarter.

Contacts have been established with outside vendors for coating substrates of AISI 1008 steel with titanium nitride, titanium boride, and iron boride. The coated materials will be tested as positive-electrode current collectors during the next quarter.

In cell wetting studies, BN felt was placed between two metal plates and immersed in molten LiCl-KCl electrolyte in a helium-atmosphere furnace well, which was then evacuated and repressurized. The felt was laterally wet by this method. Unfortunately, specimens wetted by this method which are large enough for engineering cells cracked on cooling. The problem in wetting

photo-etched stainless steel screen (used as particle retainers in FeS cells) with electrolyte was traced to the sharp corners at the ends of the holes. Treatment of this particle-retainer screen with $LiAlCl_4$ permitted the electrolyte to spontaneously penetrate the screen.

Contact angle measurements on cell materials were used to estimate the height to which a porous cell component can maintain electrolyte infiltration. For structures formed from powders with particle sizes of 100 μm or less, no problem is expected with electrolyte drainage.

A series of static corrosion tests on representative current-collector materials was conducted at 450°C in either $CuFeS_2$, NiS, NiS_2, or TiS_2 and LiCl-KCl electrolyte. These results were combined with those of similar experiments on FeS, Cu_2S, FeS_2, and CoS_2 and yielded the following order for increasing corrosiveness of the metal sulfide environments: FeS, Cu_2S, $CuFeS_2$, NiS, FeS_2, TiS_2, NiS_2, and CoS_2.

A total of 97 engineering-scale cells have undergone post-test examinations to date. The major causes of failure have been: (1) inadequate confinement of electrodes (23%), (2) metallic and/or sulfide deposits across the separators (13%), (3) separators cut by honeycomb current collectors (21%), and cause of failure not identifiable (15%). Most of the causes of cell failures are mechanical in origin and can be corrected by modifications in the cell design.

In-cell corrosion data were obtained for iron (used in Li-Al electrodes) and molybdenum (used in FeS_2 electrodes) current collectors. The corrosion of molybdenum current collectors is minimal, even in cells that operated for 400 days. The lifetime of the iron current collectors (125 μm thick) was projected to be 900 days (∿2 1/2 years) in the negative electrode.

Cell Chemistry

This effort focussed on methods to minimize or eliminate J-phase ($LiK_6Fe_{24}S_{26}Cl$) formation in FeS cells. This phase forms in the FeS electrode and causes poor cell performance. Out-of-cell tests indicated that J-phase formation should be eliminated in FeS cells by increasing the LiCl concentration in the eutectic electrolyte (58 mol % LiCl-42 mol % KCl) or by using a high operating temperature (> 450°C). Tests in small-scale FeS cells showed that a LiCl concentration of 67 mol % in the LiCl-KCl electrolyte and an operating temperature of 450°C result in a satisfactory positive electrode utilization (85% at a current density of 50 mA/cm^2).

Advanced Battery Research

The objective of this program is to devise new combinations of electrode materials and electrolytes that will provide a basis for the development of inexpensive, high-performance batteries. Recent work has focussed on development of calcium/metal sulfide cells.

A 70 A-hr sealed, prismatic $Ca(Mg_2Si)/NiS_2$ cell (assembled in the uncharged condition) was tested to evaluate the behavior of calcium-cell electrodes in a practical configuration. This cell, although not optimized for specific energy, achieved 42 W-hr/kg at the 6-hr rate. Operation was terminated after 120 cycles due to declining coulombic efficiency.

Cyclic voltammetry studies were initiated on metal disulfide (FeS_2 and NiS_2) electrodes *vs.* $CaAl_4$ in LiCl (54 mol %)-KCl (39 mol %)-$CaCl_2$ (7 mol %) electrolyte. In these studies, the high-voltage (~1.8 V) reactions of FeS_2 and NiS_2 exhibited good capacity retention during extended cycling; the reactions below 1.8 V had poor capacity retention. Cyclic voltammetry studies of the metal disulfides in other calcium-cell electrolytes will be examined.

In a search for improved negative electrodes for calcium cells, preliminary tests of Ca-Al-Zn and Ca-Pb electrodes were conducted. The Ca-Al-Zn electrode utilization was similar to that of the Ca-Al electrode; thus, zinc is not a useful addition for this electrode. Tests of the Ca-Pb electrode suggest that it is useful in stationary energy storage applications.

A search was made for an electrolyte that is less expensive than the one presently used in calcium cells (*i.e.*, 54 mol % LiCl-39 mol % KCl-7 mol % $CaCl_2$). The most suitable alternative was found to be 29 mol % LiCl-20 mol % NaCl-35 mol % $CaCl_2$-16 mol % $BaCl_2$ (mp, 390°C). The effects of this electrolyte on cell performance are now being evaluated.

I. INTRODUCTION

Lithium/metal sulfide batteries are being developed at Argonne National Laboratory (ANL) for use as (1) power sources for electric vehicles, and (2) stationary-energy-storage devices for load-leveling on electric utility systems or storage of energy produced by solar, wind, or other intermittent sources of energy. The performance and lifetime goals that are projected for prototypes of the electric-vehicle and stationary energy storage batteries were listed in the preceding quarterly report (ANL-78-21, p. 7). Future revisions of these goals may become appropriate as the requirements of these two applications are defined more specifically by systems design studies.

The present strategy for the development of the electric-vehicle battery involves the development, design and fabrication of a series of lithium/metal sulfide batteries by industrial subcontractors. Each of the batteries in this series, designated Mark I, II, and III, has a different set of objectives. The main purpose of the Mark I battery is to evaluate the general technical feasibility of the lithium/metal sulfide system for electric-vehicle batteries and to resolve interfacing problems between the battery and the vehicle and charger. The Mark II battery has higher performance goals than Mark I, but the main emphasis is on the development of designs and materials that will permit low-cost manufacturing techniques. The first phase of the Mark II program will consist of cost and design studies. The Mark III battery is planned as a high-performance prototype suitable for demonstration and evaluation in a passenger car. The performance goals for the Mark I, II, and III batteries are presented in the preceding quarterly report (ANL-78-21, p. 8).

In August 1977, a decision was made to proceed with the procurement of the first Mark I battery, which is designated Mark IA. A request for proposals was issued on November 2, and a contract was awarded to Eagle-Picher Industries, Inc. at Joplin, Missouri. This contract, which went into effect on February 22, 1978, calls for a 40 kW-hr battery package consisting of two 20-kW-hr modules to be fabricated and delivered to ANL in 12 months. The technical goals for the Mark IA battery are presented in Table I-1. In the statement of work for the Mark IA contract, the goals are listed in the following order of preference: (1) operability, (2) energy output, (3) power output, (4) specific energy, (5) specific power, and (6) lifetime.

For the stationary energy storage application, assessment studies have indicated that batteries having a life of 8 to 12 years and a capital cost of about $20 to $30/kW-hr are competitive with other methods of storing energy or producing supplemental power. The performance goals for the stationary energy storage battery are presented in ANL-78-21, p. 7. Although this type of battery must have a low cost and long lifetime, the specific-energy and specific-power requirements are less stringent than those for the electric-vehicle battery. The battery cells currently being developed for the stationary energy storage application have lithium-silicon or lithium-aluminum negative electrodes and FeS positive electrodes.

Conceptual design studies of a 100 MW-hr energy-storage plant have been underway both at ANL and at the Atomics International Division of Rockwell International.* These two conceptual designs are currently being merged into

*Under contract with ANL.

Table I-1. Technical Goals for the Mark IA Battery

Battery Characteristics	Goals
Energy Output, kW-hr[a]	40
Power Output, kW[b]	30
Maximum Weight, kg	680
Maximum Volume, liters	400
Specific Energy, W-hr/kg[a]	60
Energy Density, W-hr/liter[a]	100
Operating Temperature, °C	400-500
Maximum Heat Loss, W	400
Battery Voltage, V	144
Cycle Life[c]	200

[a]Discharge to 1.0 V/cell at the four-hour rate.

[b]Fifteen-second pulse at 50% discharge.

[c]To 20% loss of the design capacity.

one. In the present concept, the 100 MW-hr plant will consist of 5- to 6-MW-hr weatherproof modules having a modified standard-shipping container. Each battery module will consist of ∿35-kW-hr submodules, which, in turn, will be made up of eight multiplate cells. The experimental portion of this program will involve the development of a 5- to 6-MW-hr module to be tested in the BEST Facility.

The lithium/metal sulfide battery program consists of an in-house research and development effort at ANL and work performed under subcontracts with several industrial organizations. The major industrial subcontractors are Atomics International, Carborundum Co., Eagle-Picher Industries, Inc., and Gould Inc. Other subcontractors participating in the program are Budd Co., Electrical Technology Corp., ESB, Inc., ETA, Inc., General Motors Research Laboratories, ILC Technology, Illinois Institute of Technology, Sigma Research, Inc., Thermo Electron Corp., TRW, Inc., and United Technologies Corporation.

The ANL effort includes cell chemistry studies, materials development and evaluation, cell and battery development, industrial cell and battery testing, battery design, and commercialization studies. Preparations are also in progress for laboratory and in-vehicle tests of the Mark IA battery and for statistical lifetime testing of cells. Another small effort at ANL is directed toward the development of advanced battery systems that use low-cost, abundant materials.

This is the last of the current series of quarterly reports on this program. In the future, the in-house work at ANL and that of the subcontractors will be covered in annual reports for the fiscal year (October 1 through September 30). Semiannual reports for the first half of the fiscal year will be limited to the ANL in-house work.

II. COMMERCIAL DEVELOPMENT
(A. A. Chilenskas)

The objective of the commercialization studies at ANL is to provide data on the manufacturing cost and market requirements for the lithium/metal sulfide battery. The commercialization studies are conducted at ANL with assistance from industrial subcontractors and consultants. These studies involve the identification of potential markets, manufacturing cost analyses, financial plans, and evaluations of competing technologies.

A. Commercialization Studies

(W. H. Towle,* W. R. Frost, J. E. Battles, J. E. A. Graae*)

An updated estimate[1] of the manufacturing cost for Li-Al/MS_x cells, based upon current materials costs and recent cell designs, is being prepared. In addition, plans are being made to contract two or more industrial firms (probably next quarter) to conduct a design/cost study of electric-vehicle cells for the Mark II battery.

An estimate of the impact upon U. S. boron resources of the manufacture of Li/MS batteries for electric vehicles has been completed. The current U. S. production rate[2] of B_2O_3 is 6.19×10^8 kg/yr, the current cost of hydrated borate[3] is \$0.37/kg, and the current cost of ankydrous boric oxide[3] is \$0.70/kg. Table II-1 gives the world and United States reserves of B_2O_3 in 1978. Table II-2 gives the projected boron demand for conventional uses and electric-vehicle battery usage. As is shown in Table II-1, even for the period 1995-2000, when 1.75 million electric vehicles are expected to be produced, the B_2O_3 demand for use in electric-vehicle batteries is only about 5% of the projected demand for conventional uses.

Table II-1. World and United States Reserves of B_2O_3 and Ores in 1978

	Ores	B_2O_3
U.S. Reserves, (kg)	3.5×10^{11}	7.0×10^{10}
World Reserves, (kg)	1.1×10^{12}	1.7×10^{11}

*Consultants to the Chemical Engineering Division at ANL.

Table II-2. Projected Boron Demand in the U. S.

	1982-1987	1987-1991	1991-1995	1995-2000
Conventional Uses of B_2O_3[a] kg/year	7.2×10^8	8.3×10^8	9.6×10^8	1.1×10^9
Electric Car Sales, No/year	10,000	250,000	750,000	1,750,000
Li/MS Battery Production[b] MX-hr/yr	400	10,000	30,000	70,000
B_2O_3 Demand for E.V.[c] kg/yr	3.4×10^5	8.4×10^6	2.5×10^7	5.6×10^7
Total Demand, kg/yr	7.2×10^8	8.4×10^8	9.9×10^8	1.16×10^9

[a]Based upon 6.2×10^8 kg/year (1978 U.S. production rate) expanding at 3%/yr.

[b]Based on a 40 kW-hr battery/vehicle.

[c]Based upon 12.1 kg of BN felt per battery and 50% yield in the conversion of B_2O_3 to BN.

B. Systems Design

1. Design Studies for a Stationary Energy Storage Module (S. M. Zivi, T. E. Fornek*)

The objective of this study is to design an economical stationary energy storage module with a high energy efficiency. Conceptual design studies of a 5.6 MW-hr truckable battery module for this application have been conducted at ANL and Atomics International (AI);† the resulting two conceptual designs are currently being merged into one. The consolidated ANL/AI design will be used to complete a conceptual design of a 100 MW-hr energy-storage utility plant.

Work at AI also includes trade-off studies to determine the optimum cell performance relative to factors external to the cell, such as conductors, equalizing apparatus, etc. In addition, they have expanded their thermal-analysis computer code in order to study the temperature stratification on cell surfaces and internal structures.

Budd Co. is examining the feasibility of modifying the existing design of the truckable housing for the 5.6 MW-hr battery module. To reduce the cost of the housing, Budd Co. has recommended the use of a large shipping container already used in the trucking industry.

The preparation of a conceptual design for the electrical equipment in a load-leveling battery is planned. This equipment includes such items as switchgear, fuses, lightning protection, and most importantly, the conversion

*Engineering Division, ANL.

†Under contract with ANL. Also conducting related work under a contract with The Electric Power Research Institute.

equipment for the interface between the battery and the power supply. A contract for this work will probably be awarded to an industrial firm during the next quarter.

The results of earlier design efforts for the stationary energy storage module were reviewed to determine the problems that need to be addressed in the future. The problems identified were: cost of the main conductor and equalizer conductor, management of the thermal system for the battery, cell and cell-stack configuration, and technical specifications for the cells. These problems are discussed below.

A preliminary analysis was performed of radiant heat-transfer cooling, *i.e.*, using air-cooled hairpin-bend tubes in the spaces between the cell rows of a stationary energy storage battery. Our computations indicate that an economical thermal system with adequate cooling and temperature uniformity could be attained by this method.

In earlier studies at ANL, the main current conductors, along with their connectors, couplings, and fittings, were found to be a potentially large contributor to battery costs. Therefore, the effect of conductor size on battery performance was investigated. In this analysis, the optimal current density in the conductor of a series of cells with respect to the investment and operating costs dependent on conductor size was determined to be in the range of one hundred to several hundred amperes per square centimeter. The results of the conductor analysis are also being used to determine the optimum cell and cell-stack configurations.

The conductors and equipment for the charge equalizer, depending on the amount of charge needed during charge equalization, may significantly contribute to the cost of the battery. The magnitude of the equalizing charge depends on the uniformity in coulombic efficiency between the cells in the battery, on the way in which the battery cells are connected to one another, on the depth of discharge per cycle, and on the number of charge-discharge cycles between equalization charges. Thus, we are analyzing the relationship of the cost of equalization apparatus to specifications on cell uniformity, plant operating schedules, and cell and cell-stack configuration. In addition, we are analyzing the reliability of the stationary energy storage battery (or mean time between repairs) as a function of the fault-occurrence rates of the cells (*i.e.*, short circuits, open circuits) and the cell and cell-stack configuration.

2. Design Studies for Electric-Vehicle Batteries

This effort has focused primarily on the design of an insulating jacket and heating/cooling system for an electric-vehicle battery. In an effort indirectly related to the thermal management of electric-vehicle batteries, subcontracts have been awarded to Sigma Research Co. and Thermo Electron Corp. to make a conceptual design and performance analysis of a thermal energy storage system for vehicle propulsion. In other systems design work, a conceptual design for a battery charger is being developed.

a. Conceptual Design of an Insulating Jacket for an Electric-Vehicle Battery
(J. A. E. Graae, M. M. Farahat)

The electric-vehicle battery requires an inexpensive, compact, and efficient thermally insulated jacket. The use of a vacuum-foil insulated jacket is being considered for this purpose. The vacuum-foil insulation consists of multiple layers of aluminum foil. Figure II-1 shows two conceptual designs for the internal structure of a jacket for a prismatic battery: the inside of one jacket consists of corrugated metal with Min K strips* and the inside of the other jacket has a honeycomb metal construction with ceramic pins. The corrugated metal and the honeycomb metal are used to strengthen the jacket walls and the Min K strips and ceramic pins are used to prevent the jacket walls from collapsing and crushing the thermal insulation. Conceptual designs of a battery jacket without reinforcing strips or pins are also being considered. Analyses are being conducted to assess the trade-off between weight, volume, and heat loss of the battery jacket.

The Mark IA battery will be designed with a prismatic double-wall jacket. A high-quality insulation will be placed between the jacket walls. Vaccum-foil insulation made from low-emissivity metal foil separated by low-conductivity material is the best available insulation for our purposes. The heat loss through vacuum-foil insulation, depending on the number of foils and the type of foil separator, is typically less than 10^{-2} W/cm^2.

Table II-3 presents estimates of the heat loss from battery jackets with various internal structures. The goal for the jacket of the Mark IA battery is a heat loss of 400 W. The final three entries in this table all meet the Mark IA goals; however, the battery jacket design without corrugated or honeycomb metal reinforcement (the third entry of the table) requires a carbon steel case with a minimal thickness of 10 mils to avoid crushing of the vacuum-foil insulation.

*A product of Johns Mansville Co.

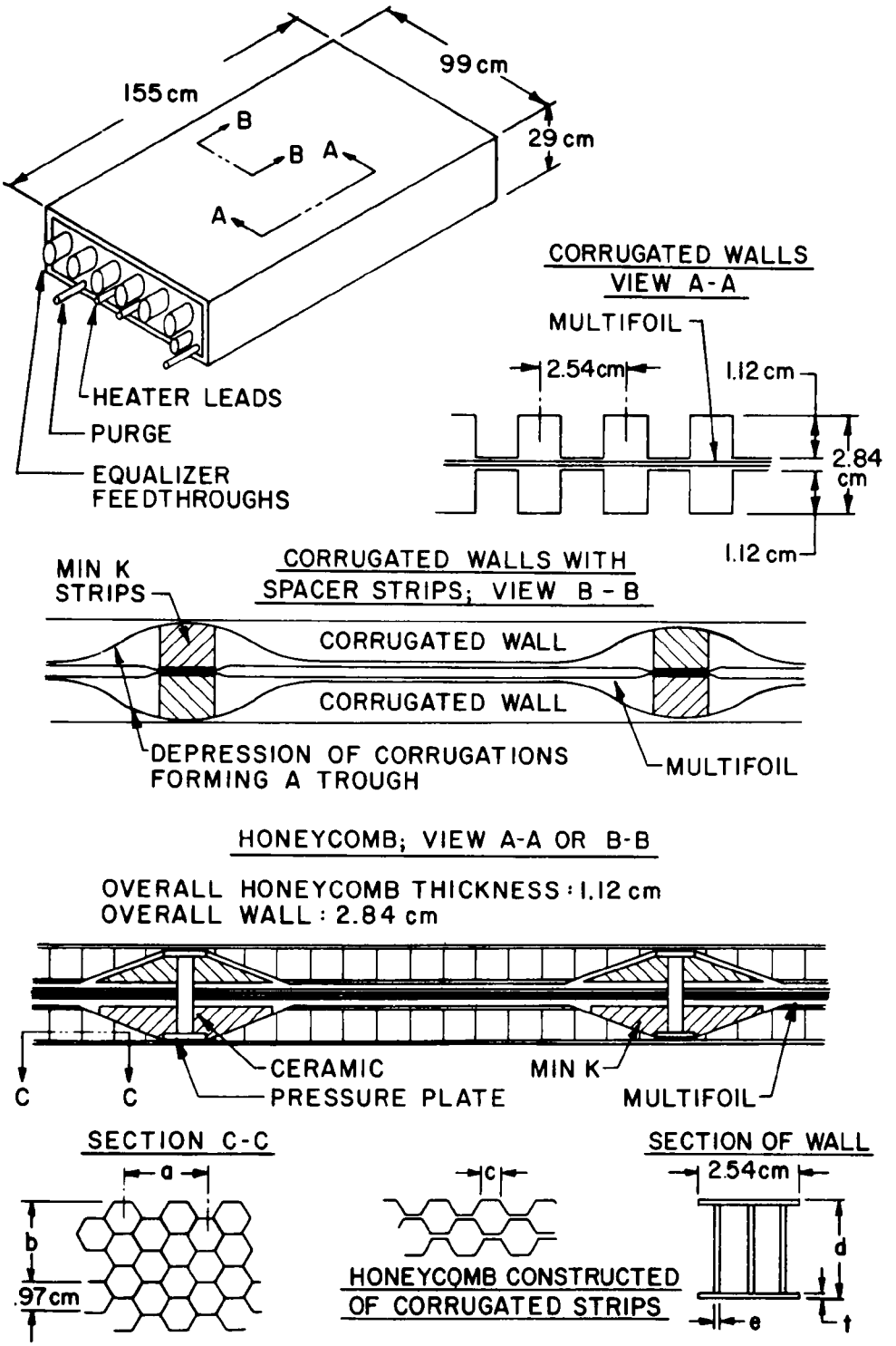

Fig. II-1. Battery Jacket Design

Table II-3. Estimated Heat Loss from Various Battery Jackets

Internal Structure of Battery Jacket	Heat Loss,[a] W
Min K strips[b] alone.	1940
Sixty layers of vacuum foil.[c]	204
Ten Min K strips and 60 layers of vacuum foil.	397
Corrugated or honeycomb sheet metal, 60 layers of vacuum foil, and Min K strips.	397
Corrugated or honeycomb sheet metal and 60 layers of vacuum foil penetrated by 44 ZrO_2 pins.[e]	316±44[d]

[a]Heat loss through plugs is assumed to be 90 W.

[b]High-compressive strength; 2 cm in width.

[c]Aluminum foil of about 3.0-μm thickness. This design is for baseline comparison.

[d]Some uncertainty in heat loss rate due to pin penetration (∿3±1 W/pin).

[e]Diameter, 0.1 cm.

b. Measurements of Heat Generation of a Cell During Cycling
(B. Zalph,* M. M. Farahat)

In any electrochemical cell, two factors lead to the evolution or absorption of heat: reversible and irreversible heating. Reversible heating ($T\Delta S$) is due to the change in entropy of active materials as they are converted from one compound to another. In secondary cells, the reversible heating must sum to zero over a complete charge-discharge cycle and is dependent only upon the rate of reaction of the active materials (assuming cell temperature is constant). Irreversible heating ($I\eta$) is strongly dependent on the current flow and is always positive (heat evolved in the cell). The total cell polarization, η, equals $I\varepsilon$ and represents the difference between the theoretical and actual cell voltage due to cell internal impedance, ε. Irreversible heating is thus proportional to I^2.

Experiments are planned to measure the heat generation in a cell surrounded by a cylindrical shell of insulation. In one experiment, the heat generation will be measured on the surface of the cell and in the surrounding insulation. The instantaneous heating rate (Q) of this cell will then be determined from the following expression.

*Student Participant, Duke University.

$$Q = M_c C_c \frac{dT_c}{dt} + M_i C_i \frac{dT_i}{dt} + K_e A_e \frac{\Delta T}{\Delta x}$$

where

M_c = mass of cell

M_i = mass of insulation

C_c = specific heat of cell

C_i = specific heat of insulation

K_e = effective one-dimensional thermal conductivity of insulation

A_e = effective conduction area

$\frac{\Delta T}{\Delta X}$ = average temperature gradient across given section of insulation

T_c = temperature of cell

T_i = temperature of insulation

In another experiment, cell voltage will be monitored during constant-current charge and discharge as a basis for determining η and the approximate fractional utilization of active materials. From these data, the reversible and irreversible heating can be determined. The information obtained from the above experiments will be used to design a heating/cooling system for the Mark IA battery.

c. Heat Generation of a 50 kW-hr Battery in an Electric-Vehicle (M. M. Farahat)

Preliminary calculations were made to estimate the temperature variation of a 50 kW-hr battery (Mark II) installed in a vehicle that is driven for 16,000 km/yr. For these calculations, two driving cycles were postulated: (1) 55 km at 40 km/hr daily for five days of the week (no driving on the weekend) and (2) 22 km at 40 km/hr daily for five days and then 160 km at 40 km/hr on the weekend. For the purposes of this analysis, we assumed no cooling or heating of the battery during driving. The other assumptions used in the analysis are presented in Table II-4.

Table II-4. Assumptions for Thermal Analysis of a 50 kW-hr Battery

Vehicle Range[a]	288 km
Battery	
Heat Loss	150 W
Weight	500 kg
No. of Cells	120
Energy per Discharge	50 kW-hr
Cells	
Ave. Voltage	1.2 V
Capacity	347 A-hr
Energy Storage	416 W-hr
Energy Efficiency	70%

[a]100% discharge.

Tables II-5 and II-6 show the temperature variations of a battery for both cycles. For the first driving cycle, the battery requires 2.9 kW-hr (at 60 W) to keep it heated over the weekend; thus the heating cost per year for this case is only $7.54 (at ¢5/kW-hr). For the second driving cycle, the battery requires almost no additional heat on Sunday; the heating cost per year for this case is less than $1.00. The energy efficiency for the batteries used in both driving cycles is high--67.4% for driving cycle 1 and 70% for driving cycle 2.

Table II-5. Driving Cycle No. 1

	Time of Day	T^a, °C
Weekday (Mon-Fri, 55 km/day)		
Start Drive	0:00	T
Complete Drive	1:54	T + 18
Start Charge	16:00	T + 3
Complete Charge	17:70	T + 13
Start New Cycles	24:00	T + 6
Weekend (Sat-Sun, 0 km)		
Start	0:00	T
Start Heating at 60 W	24:00	T + 30
Start New Cycle	24:00	T

[a]The battery operating temperature.

Table II-6. Driving Cycle No. 2

	Time of Day	T^a, °C
Weekday (Mon-Fri, 22 km/day)		
Start Drive	0:00	T
Finish Drive	0:74	T + 9
Start Charge	16:00	T - 7
Complete Charge	16:83	T - 2
Start New Cycle	24:00	T - 9
Saturday (160 km)		
Start Drive	0:00	T - 45
Finish Drive	2:00	T + 14
Start Charge	16:00	T
Complete Charge	20:50	T + 27
Start New Cycle	24:00	T + 23
Sunday (0 km)		
No Driving	0:00	T + 23
Start New Cycle	24:00	T

[a]The battery operating temperature.

d. Battery Charger Design*
(W. H. Deluca, F. Hornstra)

A charging system suitable for mass-produced electric-vehicle batteries must be economical, lightweight, reliable, and simple to use. This charger must have the capability to operate from standard power sources on a daily basis. A contract has been issued to TRW Systems to perform a design and cost study for an electric-vehicle battery (Li-Al/FeS_x) charger.

An interim progress report, received from TRW in March 1978, addressed the definition, appraisal, and selection of a battery charger conceptual design. The report included a revised set of performance specifications for the charger which were based upon a contract review meeting at ANL in February 1978. TRW recommended a charger design that was chosen from several charging schemes which met the charge-time requirements of the performance specifications. Several suggestions of means to eliminate or reduce the impact of impedances in the shunting/equalizing current were presented. On 13 March 1978, ANL suggested the shunt current-interrupt technique as the equalization scheme. One unique aspect of the equalization scheme is that it eliminates the need for voltage sense leads; therefore cell voltage can be regulated at the cell terminals. Completion of the battery charger design is expected by the end of April.

*Funded by Department of Energy, Division of Transportation Energy Conservation.

III. INDUSTRICAL CELL AND BATTERY TESTING
(W. E. Miller, E. C. Gay)

Testing of industrially fabricated lithium-aluminum/metal sulfide cells is continuing. The improvements in cell designs that are demonstrated by this testing will be incorporated into future industrial cells. Fabrication of equipment for testing cells and batteries continues. This equipment includes a facility to test large-scale (up to 60 kW-hr) batteries and another facility to test up to 100 industrial cells.

A. Testing of Contractor Produced Cells

Two industrial firms under contract with ANL--Eagle-Picher Industries, Inc. and Gould Inc.--are fabricating Li-Al/FeS and Li-Al/FeS_2 cells. These cells are being tested either at ANL or in their own laboratories. A performance summary of the Eagle-Picher and Gould cells operated during this quarter is presented in Appendix A.

The Atomics International Division of Rockwell International is continuing to fabricate and test Li-Si/FeS_x cells under a subcontract with ANL.

1. Qualification Testing of Eagle-Picher Cells
(T. D. Kaun, P. F. Eshman, W. A. Kremsner)

The qualification testing of Eagle-Picher cells is continuing. The designs of these cells were basically the same as those of the baseline FeS and FeS_2 cells (ANL-76-98, pp. 14-15), but with carefully selected variations (ANL-77-75, pp. 17-18). These variations included electrode thickness, capacity loading, separator material, position of the positive terminal rod, diameter of the positive terminal rod, and design of the positive current collector. The modified cells are evaluated using a standardized procedure that permits a comparison of the performance characteristics of cells with different designs.

Eagle-Picher recently completed the fabrication of 14 Type I-8 cells. These cells were built to produce improved versions of the Type I-7 cells* (ANL-77-75, p. 68), which had attained the best performance of any previous industrial cells. In the Type I-8 cell design, the zirconia cloth particle retainer normally used on the positive electrode of their cells was eliminated or replaced with 100-mesh molybdenum screen. The particle retainer for the negative electrode of the Type I-8 cell was eliminated or else 165-mesh molybdenum screen was used.

After filling the Type I8 cells with electrolyte, their "frozen" (*i.e.*, room temperature) resistance was found to range from 0.1 to 3×10^6 Ω. An attempt was made to operate one of the low-resistance cells, but this effort failed because of poor coulombic efficiency.

---

*Essential features of this design: very dense FeS_2 positive electrode (1.36 A-hr/cm^3) and a flexible connection between the terminal rod and current collector.

Eagle-Picher then examined several of the Type I-8 cells, both cells that had been cycled and cells that had not been cycled. They concluded that particulate material had escaped from both the positive and negative electrodes during the electrolyte-filling operation.

As a result of their experience with these cells, Eagle-Picher has taken the following corrective actions: the active materials were carefully screened to eliminate fine particle sizes and Y_2O_3-felt particle retainers were used under the molybdenum screens on both the positive and negative electrodes. Some of the new Type I-8 cells will be subjected to vibrational tests.

Attempts were made to cycle a number of the faulty Type I-8 cells at ANL, namely, I-8-H-027, I-8-K-032, and I-8-K-033* (molybdenum screen particle retainers). These cells exhibited poor coulombic efficiency and short-circuited after less than 48 cycles. Another Type I-8 cell, I-8-L-034,* built with no particle retainers at all, had a frozen resistance of about 3×10^6 Ω. This cell was cycled at charge and discharge currents of 3 A (10 mA/cm^2) for two cycles, and attained 95% utilization of the positive electrode. Subsequent utilization of 66.4%, 61.8%, and 56.4% were achieved at discharge current densities of 40, 60, and 80 mA/cm^2, respectively (the Type I-7 cell had utilizations of 55.0%, 52.4%, and 50.9% at discharge current densities of 40, 60, and 80 mA/cm^2, respectively).

Qualification testing demonstrated a specific energy of 90 W-hr/kg at the 4-hr rate (Fig. III-1), which is higher than that of the Type I-7 cell (ANL-78-75, p. 18), and a peak specific power of 65 W/kg (Fig. III-2). This cell also achieved a low resistance, 6.5-7.5 mΩ, which was attributed to the positive current collector design. Although the cell short-circuited within 20 cycles, probably due to poor electrode particle retention, it had the best performance of any Eagle-Picher cell produced to date.

Investigations by the Cell Chemistry Group indicated that FeS cell performance can be improved by the addition of LiCl to LiCl-KCl eutectic electrolyte. Thus an Eagle-Picher FeS-Cu_2S cell, namely, 1A5, was operated to assess the effect of LiCl-rich electroylyte (67 mol % LiCl-33 mol % KCl) on performance. This cell had the same design as that of Cell 1A6 (75-A-hr theoretical capacity),† which operated for 96 cycles (66 days) without a decline in performance. Operation of Cell 1A5 was terminated after 43 cycles (19 days) due to a short circuit in the electrical feedthrough. The specific energies and the peak specific powers of both these cells were nearly identical--47 W-hr/kg at the 4-hr rate and 45 W/kg, respectively. Positive electrode utilizations (75 A-hr, theoretical capacity) were 70% at a current density of 40 mA/cm^2, 66% at 65 mA/cm^2, and 47% at 130 mA/cm^2. The LiCl-rich electrolyte changed the shape of the cell's discharge voltage curve. Two distinct voltage plateaus were exhibited instead of one. However, the average voltage was unchanged. This alteration of the voltage curve may be associated with suppression of J-phase formation. Overall, no improvement of cell performance

*These cells had higher negative-to-positive capacity ratios than those of the Type I-7 cells (1.3 *vs.* 1.0).

†This cell was reported in ANL-77-68, p. 60.

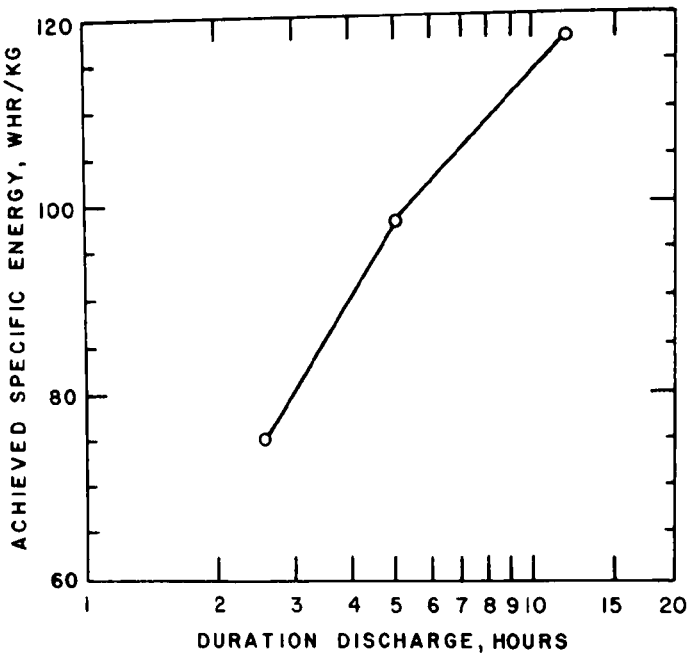

Fig. III-1.

The Specific Energy of Cell I-8-L-034

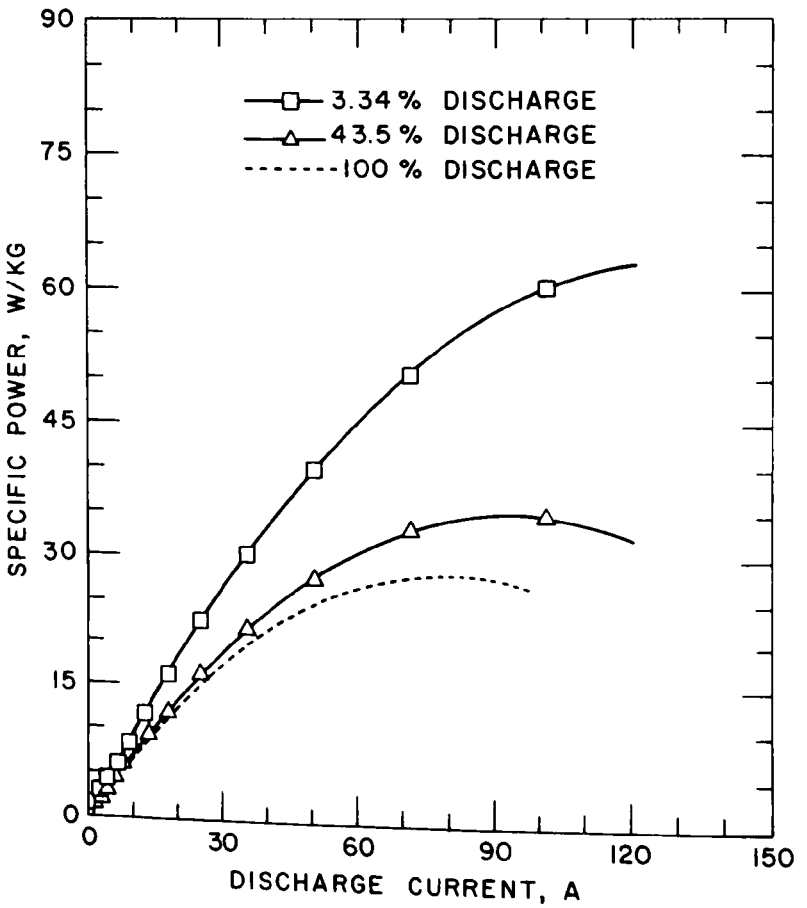

Fig. III-2.

The Specific Power of Cell I-8-L-034

could be attributed to the use of a LiCl-rich electrolyte in an FeS-Cu_2S cell; however, the effect of LiCl-rich electrolyte of the performance of an engineering-scale FeS cell remains to be determined.

2. Other Tests on Eagle-Picher Cells
(V. M. Kolba, J. L. Hamilton, G. W. Redding)

Tests were conducted on Eagle-Picher cells to evaluate the effect on performance of various charging currents and elevated operating temperatures.

a. Operation of Cells at Elevated Temperatures

The effect on performance of operating four Li-Al/FeS-Cu_2S cells--1B4, I-3-C-1, I-3-B-2, and I-3-C-3 (see Appendix A for a detailed description of these cells)--at elevated temperatures (up to 525°C) was continued during this quarter. The effect on capacity of raising the operating temperature of these cells from 425 to 500°C (or 525°C) and then returning the temperature to 425°C is presented in Table III-1. A plot of capacity *vs* operating temperature for Cell I-3-C-2 is given in Fig. III-3. As can be seen from Table III-1, all four cells had better capacities after the operating temperature was raised from 425 to 525°C and returned to nearly the same capacity after the temperature was reduced to 425°C. There appears to be some residual effect on cell capacity after the high-temperature operation. Operation of Cell I-3-C-2 has been terminated on cycle 527 because of poor performance, and cell IB4 has decreased in coulombic efficiency. Cells I-3-B-2 and I-3-C-1 continue to perform well.

Table III-1. Capacity of Four FeS Cells at Various Operating Temperatures

	Cell Capacity,[a] A-hr			
Operating Temp, °C	1B4	I-3-B-2	I-3-C-2	I-3-C-1
425	61 (40)	95	62	47
450	[b]	[b]	92	63
475	[b]	[b]	100	[b]
500	91 (72)	105 (92)	103	95
525	[b]	[b]	104	[b]
450	61 (32)	87 (74)	63	[b]
425	[b]	[b]	56	70

[a]Measured at 10-A current. Numbers in parenthesis indicate capacity at 15-A current.

[b]No measurement available at this temperature.

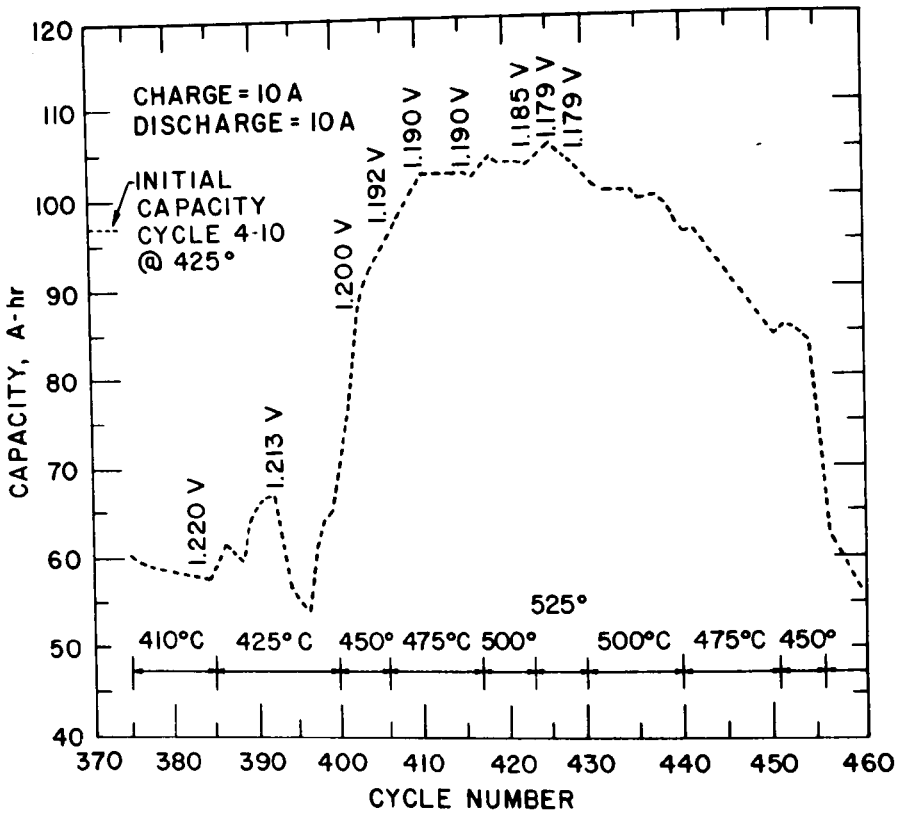

Fig. III-3. Effect of Cell Temperature on Capacity of Cell I-3-C-2

b. Cell Voltage as a Function of State of Charge

Cell I-3-C-1 was also used to determine the open-circuit voltage as a function of state of discharge.

This cell was operated at 450°C and a charge-discharge current of 10 A to a discharge cutoff voltage of 1.0 V in order to measure the "normal" deep discharge capacity. On the next cycle the cell was discharged to 5% of this capacity and then left on open circuit for one hour after which the open-circuit voltage was measured. Next the cell was discharged another 20% and the same procedure was followed to obtain the open-circuit voltage at 25% discharge. The open-circuit voltages at 50, 75, and 100% of the normal discharge capacity were also obtained by the same method. The above procedure was completely repeated with the cell at 500°C.

At 450°C (500°C) the normal discharge capacity was 63 A-hr (97 A-hr); under the interrupted current conditions, the capacity of the incremental discharges added up to 10% (7%) more than the normal capacity. As can be seen in Fig. III-4, the open-circuit voltage changes considerably at discharge capacities of 20 to 50 A-hr. Above discharge capacities of 50 A-hr, the change in voltage is more gradual.

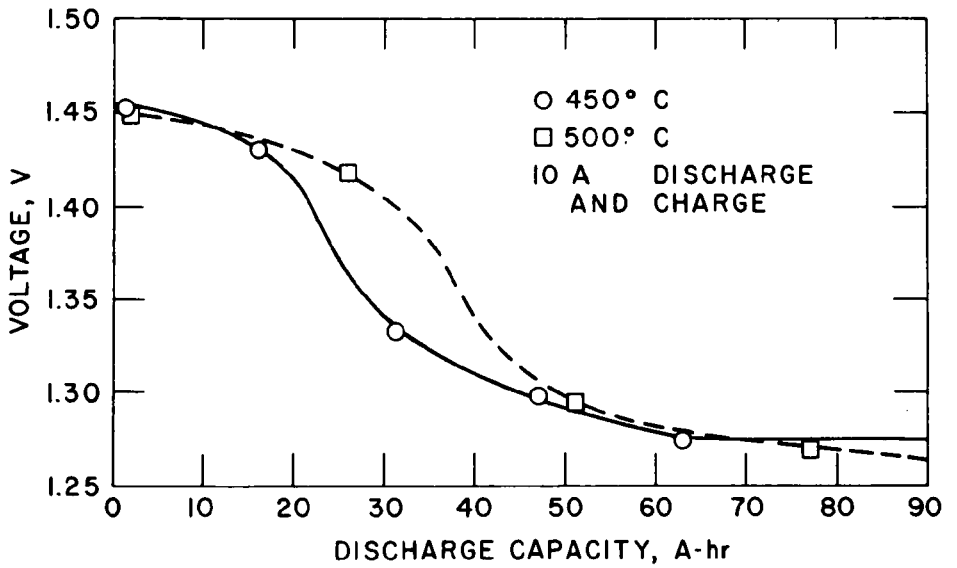

Fig. III-4. Open Circuit Voltage (at 1 hr) *vs* State of Discharge for Cell I-3-C-1

3. Qualification Testing of Gould Cells
(T. D. Kaun, P. F. Eshman, W. A. Kremsner)

Gould Inc. is fabricating 55 upper-plateau* FeS_2 cells under a subcontract with ANL. The Gould cells consist of hot-pressed (13 x 18 cm) electrodes that are assembled in the uncharged state. These cells are being tested to determine the effect on performance of (1) current-collector design, (2) lithium content in the negative electrode, (3) electrolyte volume and thickness in the positive electrode, and (4) method of particle retention. The following mode for testing Gould cells was established by both ANL and Gould: discharge current densities of 33, 66, and 100 mA/cm^2 with a discharge cutoff voltage (IR-free) of 1.3 V, and a current-limited (33 mA/cm^2), constant-voltage (2.2 V) charge. This cycling mode is expected to provide data for determining the optimum electrode design of this type of cell. A seven-day cycling schedule (computer controlled) was selected for these tests. Graphs of voltage *vs.* capacity, specific energy *vs.* discharge rate, and specific power *vs.* discharge rate are made for each cell.

A number of the Gould cells have been qualification tested. Performance data on 15 such cells, presented in Table III-2, indicate that cells of similar design have higher utilization of the active material when the charged negative electrode contains 50 mol % rather than 45 mol % lithium. With an electrode thickness of >5.6 mm, the capacity usually decreased with increasing current densities.

Four of the Gould cells with 5.6-mm thick positive electrodes (namely, G-04-03A, -005, -11A, and 017) had 25-28 mol % lithium in the negative electrode after discharge and four cells with 10.4-mm thick positive electrodes (namely, G-04-09A, -13A, -14B, and -19A) had about 30 mol % lithium after discharge, regardless of the fully charged composition or the assumed utilization of the negative electrode. A common composition in the discharged state of the negative electrode regardless of the amount of lithium loaded indicates that the capacities of cells with high assumed negative utilizations were limited by the negative electrode.

Since the negative electrode appears to limit capacity in some of the Gould cells, an assessment of the upper-plateau FeS_2 cell performance is difficult at this time. Nonetheless, high utilizations of upper-plateau capacity have been achieved. For example, Cell G-4-010 showed >85% utilization at a current density of 100 mA/cm^2 (45 A). In Fig. III-5 the voltage-capacity curves for this cell reveal only slight electrode polarization for increasing current. Although not optimized for energy density, Cell G-04-010 achieved a specific energy of 75 W-hr/kg at the 4-hr rate and cell G-04-03A achieved a peak specific power of 75 W/kg.

---

*These cells are operated only on the upper of two voltage plateaus that are characteristic of FeS_2 cells.

Table III-2. Performance Data on 15 Gould FeS_2 Cells

Gould Cell No.	Pos. Electrode Thickness, mm	Pos. Electrode Theo. Capacity,[a] A-hr	Assumed Neg. Utilization,[b] %	Neg. Comp., mol % Charged	Neg. Comp., mol % Discharged	Cell Capacity, A-hr 33 mA/cm^2	Cell Capacity, A-hr 67 mA/cm^2	Cell Capacity, A-hr 100 mA/cm^2	Cell Capacity, A-hr 133 mA/cm^2	Cell Resistance, mΩ
G-04-002	8.0	138.6	65	50.0	31.1	121	114	110	102	5.0
G-04-03A	5.6	96.1	75	50.0	28.6	82	81	81	81	5.5
G-04-005	5.6	96.1	75	50.0	28.6	71	71	71	70	5.0
G-04-09A	10.4	181.1	65	50.0	30.2	164	139	126	150	6.0
G-04-010	10.4	186.1	75	50.0	25.5	165	159	152	d	7.5
G-04-11	5.6	96.1	65	45.2	28.0	81	80	80	c	6.6
G-04-012	8.0	138.6	65	45.2	28.2	116	113	113	c	8.5
G-04-13A	10.4	181.1	65	45.2	30.6	134	128	126	c	8.0
G-04-014	10.4[d]	154.8	65	45.2	c	125	117	107	105	7.5
G-04-14B	10.4[d]	146.1	65	45.2	30.2	112	110	106	c	6.0
G-04-017	5.6	96.1	65	45.2	26.8	86	86	87	86	5.6
G-04-19A	10.4	181.1	65	45.2	30.6	129	135	137	c	8.5
G-04-022	10.4[d]	149.8	65	45.2	c	136	135	135	134	12.0
G-04-023	5.6	97.5	65	45.2	c	77	71	69	c	13.5
G-04-025	10.4	178.0	65	45.2	c	130	130	133	c	10.0

[a] Upper-plateau capacity.

[b] Negative-to-positive capacity ratio increases as assumed negative utilization decreases.

[c] No data available yet.

[d] The porosities of these electrodes are 35%; all other cells have positive electrode porosities of 30%.

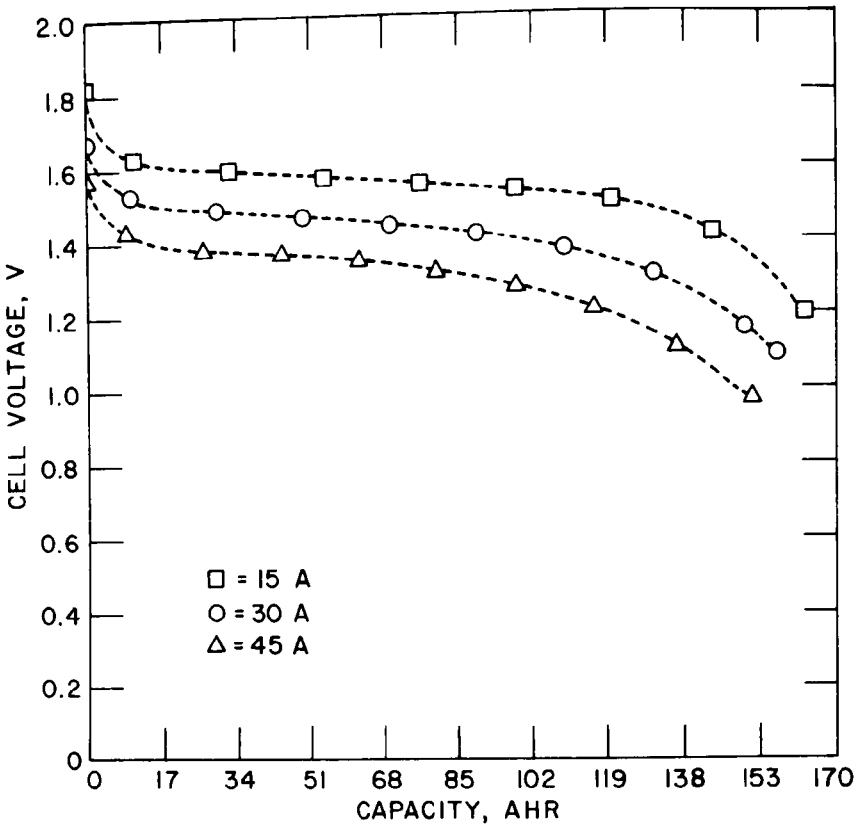

Fig. III-5. Voltage *vs.* Capacity Curve for Cell G-04-010

4. Lifetime Testing of Gould Cells
(V. M. Kolba, J. L. Hamilton, G. W. Redding)

The performance of Cell G-04-013 (upper-plateau FeS_2 cell) was stable after 68 cycles of operation. Therefore, this cell was selected for lifetime testing to determine the rate of capacity decline during long-term cycling. After 51 more cycles (total lifetime, 119 cycles), the coulombic efficiency declined from 97 to 93%.

Operation of the FeS cell G-1-03-002, which had $CaCl_2$ added to the electrolyte in the negative electrode, was resumed to determine the effects of cycling on this type of cell. After 45 additional cycles (total, 133 cycles), the coulombic efficiency declined from 98.8 to 89%.

5. Tests on Atomics International's Cells

A load-leveling cell with a capacity of 2.5 kW-hr, designed and built in FY 1977, was placed in operation.* This cell contains 16 electrode pairs with each electrode measuring approximately 23 x 23 cm. The active materials are $Li_{4.5}Si$ and FeS when the cell is fully charged. After completion of 15

*All cell tests performed at AI.

cycles, a capacity of 2.24 kW-hr was recovered at about the 10-hr rate. Immediately thereafter, the cell short-circuited during discharge. The location of the short circuit was determined, the two faulty sets of electrodes were jumpered out, and the cell was again placed in operation. Shorting was again observed after a total of 35 cycles and operation was terminated. The cause of the short circuit will be investigated.

A series of bicells with electrodes measuring 12.7 x 17.8 cm were built and tested as electric-vehicle cells. The active materials used were the same as those used for the 2.5 kW-hr cell. Improvement in high-rate performance by the use of LiCl-rich electrolyte was demonstrated. This finding is consistent with work performed at ANL showing that J-phase formation is inhibited by the use of this non-eutectic electrolyte. The feasibility of replacing honeycomb negative electrode structures with potentially less expensive shelf structures was successfully demonstrated.

B. The Mark IA Battery

(V. M. Kolba)

Eagle-Picher Industries has been awarded the Mark IA battery contract. This contract entails the development, design and fabrication of a 40 kW-hr battery by early 1979. The battery will undergo stationary and in-vehicle testing at ANL (see following section).

The statement of work calls for a 40 kW-hr battery package consisting of two 20 kW-hr modules. The energy storage capability is to be greater than 40 kW-hr at the 4-hr rate after 60 equivalent deep discharges, and the power is specified as 30 kW for a 15-second pulse at a 50% state of charge. The maximum weight of the Mark IA battery is 680 kg and the maximum volume is 400 L. The operating temperature will be between 400 and 500°C, with a maximum heat loss of 400 W. See Table III-3 for a more detailed description of our operation criteria for this battery. The battery cells are expected to be of a multiplate design employing Li-Al negative electrodes and FeS positive electrodes with molten LiCl-KCl electrolyte.

Table III-3. Operation Criteria for Mark IA Battery

Energy Storage[a]	>40 kW-hr after 60 deep discharges
Power[b]	30 kW
Specific Energy[a]	60 kW-hr/kg through 60th cycle
Operability	4 months without failure
Lifetime	>200 cycles without loss of more than 20% of designed energy storage
Heat Loss	400 W
Nominal Battery Voltage[c]	144 V
Battery Volume	400 L

[a] Four-hour rate.

[b] Fifteen-second pulse; 50% discharge.

[c] Average voltage.

C. Equipment for Cell and Battery Tests

A facility for testing up to 100 industrial cells is presently being constructed at ANL; to be included as an integral part of this facility is a computer system for monitoring of cell performance and data acquisition. This facility will be used primarily for lifetime testing of industrial cells. A facility is also being constructed for laboratory tests of large-scale (up to 60 kW-hr) electric-vehicle batteries that will precede in-vehicle tests. This facility will have the capability for computer-controlled operation and data acquisition. In addition, equipment for in-vehicle testing of batteries is presently being designed.

1. Stationary Testing Facilities for Batteries

(V. M. Kolba, G. W. Redding, J. L. Hamilton, W. W. Lark, C. Swoboda G. Chapman, R. Smith,* J. Thomas,† P. Cannon,† S. D. Gabelnick‡)

Robicon power supplies for the stationary testing facility for batteries (up to 60 kW-hr) are scheduled for delivery in April 1978. Procurement of the water chillers for these units has been initiated. Because of the change from FeS_2 to FeS cells for the Mark IA battery, the original design of the laboratory equalizer needs to be modified to permit equalization of 120 instead of 100 cells, and the power supplies have to be modified for charge regulation of 1.6 instead of 2.1 V (full charge voltage). Tests** have been conducted to establish the modifications required to permit use of the present power supplies with FeS cells. The computer-controlled operation for the stationary battery test facility will use Digital Equipment Corporation's RT (Real Time)-11. This system is capable of running one data-acquisition task in the foreground (high priority) and data analysis and display tasks or a series of such tasks in the background (lower priority). A configuration of the system software for supporting our hardware (known as a "system generation" or "sysgen") was prepared on a PDP 11/70 computer. A Fortran compiler and library were installed and tested as well.

All of the components for computer-controlled data aquisition have been received and checked out, and a computer to CAMAC†† interface has been established. Some of the computer software from the National Battery Testing Laboratory (NBTL) is being adapted for this facility. A CAMAC checkout routine was obtained from Kinetics System and will be used to check out the computer hardware.

---

* Electronics Division of ANL.

† Applied Mathematics Division, ANL.

‡ Chemical Engineering Division, ANL.

** By W. H. Deluca of Chemical Engineering Division, ANL.

†† The Computer Automated Measurement and Control System is an established international control-system standard.

2. Lifetime Test Facility for up to 100 Cells
(J. D. Arntzen, V. M. Kolba, W. E. Miller)

Construction is under way on a facility to test large numbers of cells supplied by industrial contractors, and to provide statistical information that will be useful for evaluating cell and battery designs and fabrication techniques. Originally, the facility was planned to accommodate 100 cell testing stations; however, because of budget restrictions, only 50 stations for cell testing are being initially constructed.

The open relay-rack frames which form the individual cell-test stations have been received, assembled, and installed. Cable trays for input wiring to the data-acquisition system (DAS) are in place. The wiring of the control panels has been completed and the panels have been installed in the individual test stations. Corrections of some minor difficulties with the prototype cycler constructed by the ANL Electronics Division (ANL-78-21, p. 29) were completed and bids were solicited for the manufacture of 50 units.

A prototype furnace module was assembled, and thermal tests were conducted. At approximately 80% of rated power, the furnace was brought to cell operating temperature (460°C) in less than one hour. Temperature was held at 460°C for more than 4 days with a power consumption of less than 130 W. The furnace was shut off and allowed to cool. The time required for the furnace to cool from 460 to 50°C was in excess of 48 hr, thus indicating excellent insulation. Examination of all furnace components revealed no damage or deterioration in any location. Construction of 50 furnace units is under way and approximately 70% complete.

Power supplies for the 50 furnace modules have been ordered, with delivery of 25 units scheduled for May 19 and the balance due on May 26. piping for the argon cover gas for the furnaces has been requested, and should be installed by the middle of May. Construction of the enclosure for the data-acquisition system should be concluded by the middle of April, and the components for the data-acquisition system should be delivered during June.

3. Equipment for Testing Batteries in Vehicles

a. Preliminary Tests Using a Renault Electric Vehicle
(E. R. Hayes, A. A. Chilenskas)

Preliminary road tests on a Renault electric vehicle (lead-acid batteries) have been completed. The total weight of the vehicle is 860 kg (1892 lb), and the motor output is 5.25 kW (7 hp). The battery alone weighs 344 kg (757 lb) and has an output of 72 V. The road tests were conducted according to DOE recommendations and will provide baseline data for the testing of lithium/iron sulfide batteries in vehicles.

The steady speeds selected for the Renault were 40 km/hr (25 mph) and 24 km/hr (15 mph). An ambient temperature difference of 15°C resulted in a less than 10% difference in the 40 km/hr range test. Since the test track was not level, the "end-of-range" was the last level spot of the road at which the car maintained the required speed. The in-vehicle battery test approximated an SAE 227a Schedule "B" cycle test.[4] However, the exact

test could not be performed because the test track at ANL has five intersections that interfere with maintaining the constant vehicle velocity required by the "B" cycle.

These tests showed that this vehicle* could travel on a level road for 145 km at a constant speed of 24 km/hr, for 88 km at a constant speed of 40 km/hr, and for 74 km at variable speeds. The vehicle energy economy† was 0.27 kW-hr/km at a constant speed of 40 km/hr and 0.33 kW-hr/km at variable speeds. The acceleration of this vehicle on a level road was 0-20 km/hr in 2.1 sec, 0-40 km/hr in 7.0 sec, and 0-56 km/hr in 21.8 sec. The power required to overcome rolling resistance and aerodynamic drag was 1.51 kW at 20 km/hr and 3.89 kW at 40 km/hr. On grades of 2.2, 11.2, and 25.2%, the maximum speeds that could be attained were 52 km/hr, 35 km/hr, and 20 km/hr, respectively.

The Robicon Battery Cycler is being used to characterize the lead-acid battery used in the Renault. The test information includes capacity *vs.* voltage at selected discharge rates, peak power *vs.* depth of discharge, capacity *vs.* constant-power discharge, and internal resistance *vs.* depth of discharge. These tests will permit us to compare a lead-acid battery with a Li-Al/FeS battery under laboratory conditions and will provide data for evaluating the performance of the lithium/metal sulfide battery under test conditions.

Substitution of one 6-V lithium/metal sulfide battery module for one of the 6-V lead-acid battery modules in the Renault is planned for the first in-vehicle test of the advanced battery. In addition, during these tests we will evaluate the road-worthiness of the battery case and the reliability of the on-board testing instruments (see below).

b. On-Board Instrumentation
(W. H. Deluca, E. R. Hayes, F. Hornstra, A. A. Chilenskas)

An electric van will be procured in FY 1978 to serve as a test bed for road testing the Mark IA battery. Initially, baseline data will be acquired with lead-acid batteries by road testing this vehicle. The Mark IA battery will then be installed in the vehicle and road-tested. An instrumentation package is presently being developed to measure and record vehicle and battery performance during operation. Preliminary equipment specifications have been outlined, and various manufacturers and users of electric vehicle testing equipment have been contacted to obtain relevant information. Particularly useful have been site visits to the Jet Propulsion Laboratories of NASA/Lewis, and the AMOCO Research Center in Naperville, Illinois. Existing instrumentation technology and components will be used in the ANL design whenever possible.

A general outline of the computer-controlled data-acquisition and data-analysis system for the vehicle is given in Fig. III-6. During vehicle operation, the data-acquisition system measures and records various

---

*Batteries fully charged.

†AC power measured at the input to the battery charger.

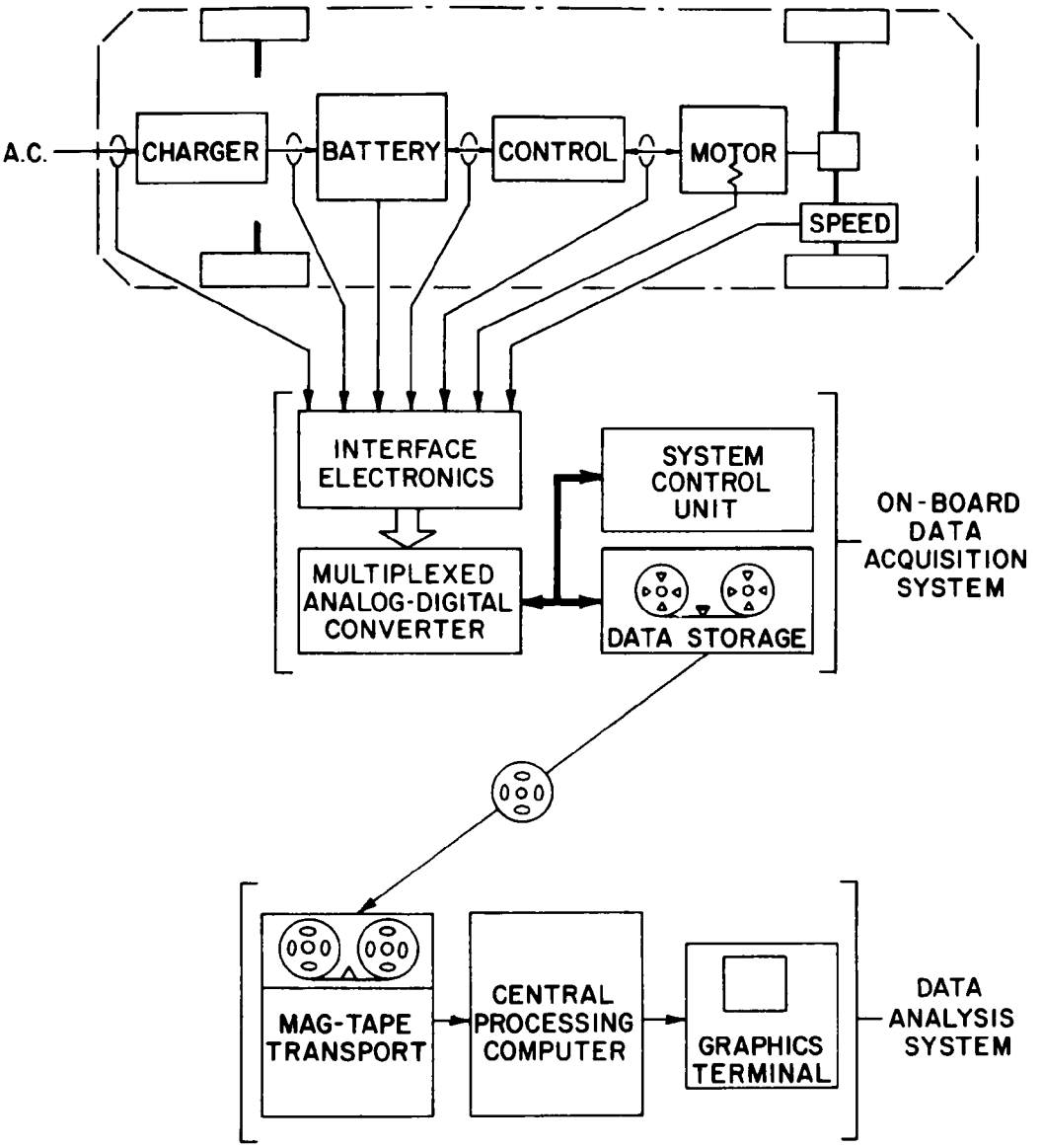

Fig. III-6. Block Diagram of Data-Acquisition and Processing Systems for In-Vehicle Battery Performance Evaluation.

battery and vehicle parameters, and permits performance evaluation when processed into the data-analysis system. All of the parameters to be monitored require signal conditioning or isolation electronics. This is necessary to match the transducer or sense-point-voltage signal to the input range of the analog-to-digital converter. Isolation electronics provides noise signal rejection and allows the data system to electrically "float" (*i.e.*, to be electrically isolated from the vehicle chasis and propulsion system). The analog signals from the battery and vehicle will be converted to digital values and stored on magnetic tape in a format suitable for direct playback into the computer for analysis. The system control unit is a microprocessor that executes preprogrammed command functions which are stored in local read-only memory. This unit will determine the sampling rate and which signals to sample and record. At present, discussions are being held with various manufacturers of microprocessor equipment to outline an instrumentation package that provides data acquisition with the possibility of future modifications as the program develops.

The data-analysis system is used to process the recorded data from the in-vehicle test and present the results in various output formats. For ease of interpretation, output results will be graphically displayed. Present plans are to use the central computing facility at ANL to minimize the programming effort required for data processing and display.

IV. CELL DEVELOPMENT AND ENGINEERING
(E. C. Gay and H. Shimotake)

The effort in this part of the program is directed toward the development of Li-Al/FeS_x cells capable of meeting the requirements for electric-vehicle and stationary energy storage applications. Recent cell development work has concentrated on improving lifetime and specific energy at high discharge current densities (>100 mA/cm^2). Whenever advances in cell technology are demonstrated at ANL, these advances are incorporated as quickly as possible into the industrial cells.

During this quarter, various changes were made in the positive electrode composition, the electrolyte composition, and the cell operating temperature to determine the effect of these cell modifications on the performance of Li-Al/MS_x cells. The use of MgO powder separators in FeS cells continues to be tested.

A. Development of FeS Cells

In the past, two types of metal sulfides have been used as the active material in the positive electrode--FeS and FeS_2. The FeS_2 electrode is capable of high specific energy and specific power, but has the disadvantages at present of limited lifetime and the requirement for expensive current-collector materials. Consequently, the FeS electrode has been selected for the first electric vehicle battery (Mark IA). Efforts are currently under way to develop an FeS cell that meets the performance goals for the Mark I battery.

1. Uncharged Cells with Pressed Electrodes
(L. G. Batholme)

Cell chemistry studies (ANL-77-35, p. 57) indicated that the formation of J phase ($LiK_6Fe_{24}S_{26}Cl$) in FeS electrodes has an adverse effect on the electrode kinetics. Previous results also suggested that J-phase formation can be avoided or minimized by adding Cu_2S to the FeS electrode or by increasing the LiCl content of the electrolyte. Thus, three engineering-scale FeS cells were tested to determine whether or not these modifications in the FeS cell effect utilization. Cell R-34 had 16 mol % Cu_2S added to the positive electrode and eutectic electrolyte (58 mol % LiCl), Cell R-37 had no copper additive and eutectic electrolyte, and Cell R-38 had no copper additive and LiCl-rich electrolyte (61 mol % LiCl). All three cells were assembled uncharged, had hot-pressed electrodes, and were limited in theoretical capacity by the positive electrode.

As can be seen in Fig. IV-1, the utilization of the positive active material in Cell R-38 is significantly higher than that of Cell R-37 and the utilization of Cell R-38 is lower than that of Cell R-34. Thus, of the three cells, the one with Cu_2S added to the positive electrode has the best utilization. The long-term effects of operating FeS cells with LiCl-rich electrolyte or 16 mol % Cu_2S in the positive electrode are yet to be determined.

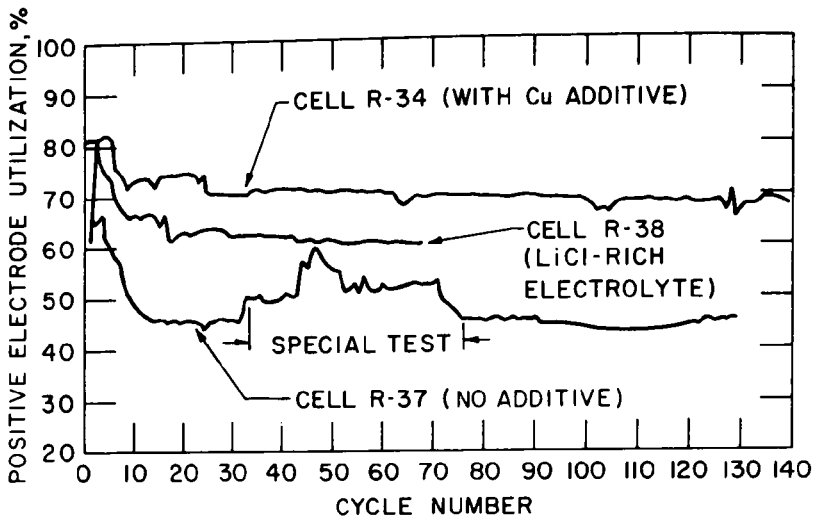

Fig. IV-1. Utilization of Three R-Series Cells

2. Charged FeS Cells with Pressed Electrodes
(F. J. Martino)

Charged engineering-scale cells, designated "M-series", were designed as compactly as state-of-the-art technology permits. In addition, BN felt separator/retainers were used in these cells. The design of this cell is pictured in ANL-78-21, p. 35.

During this quarter, two M-series cells with FeS electrodes were put into operation. The first one, M-6, had the same active material and electrolyte as Cell R-34. This electrode composition and electrolyte were chosen for Cell M-6 because of the excellent utilization achieved by R-34 (see Fig. IV-1). The initial performance of Cell M-6 was as follows: positive electrode utilization,* 64% at a current density of 74 mA/cm^2; specific energy, 54 W-hr/kg at a current density of 74 mA/cm^2; cell resistance, 4-5 mΩ; and specific power, 78 W/kg at 100% charge and 52 W/kg at 50% charge. After the operating temperature was increased from 450 to 500°C,† the positive electrode utilization of Cell M-6 increased by 24% and the specific energy by 37%; however, the cell resistance and specific power remained unchanged. Operation of this cell was voluntarily terminated after 64 cycles and 44 days.

The other M-series cell, M-8, was built with the same active materials and LiCl-rich electrolyte as Cell R-38. At present, this cell has been operating for 10 cycles at 450°C. Preliminary data showed a positive electrode utilization of 64% (72 A-hr) and a specific energy of 56 W-hr/kg at a current density of 74 mA/cm^2. The cell resistance is 3.5-4.0 mΩ.

---

*The positive electrode of Cell M-6 limited cell capacity.

†Previous studies (ANL-78-21, pp. 21-24) had shown that operation at 500°C improves performance.

3. Small-Scale FeS Cells
(K. E. Anderson, D. R. Vissers, T. Ho*)

Investigations of additives to the positive electrode of small-scale Li-Al/FeS cells were continued. Three small-scale cells were constructed with the following additives to the positive electrode: no additive, 10 wt % Cu_2S, and 11 wt % CoS. The preliminary results indicate that the utilization of an FeS electrode is increased by the addition of Cu_2S and not significantly affected by the addition of CoS.

To determine the effect of electrolyte composition on positive-electrode utilization, the following four LiCl-KCl electrolyte compositions were tested at 450°C in a small-scale FeS cell (LiCl content in wt %): 44, 47 (eutectic), 51, and 54. The liquidus temperatures of the four electrolyte compositions are 350, 375, 400, and 425°C, respectively. The positive-electrode utilization of the FeS cell with eutectic electrolyte was 50%. The utilization of this cell increased by 60% when 54 wt % LiCl was used, and by 30-50% when 47 or 51 wt % LiCl was used in the electrolyte. Another small-scale FeS cell was constructed with KCl-rich electrolyte (39 wt % LiCl; liquidus, 415°C). Testing of this cell showed that the positive electrode-utilization was 50% less than that of the FeS cell with eutectic electrolyte.

4. Multiplate Cell Design
(H. Shimotake)

In order to increase the specific energy of the Li-Al/FeS cell to meet the goals for the Mark I and II batteries (>100 W-hr/kg at the 4-hr rate), a multiplate cell (Fig. IV-2) has been proposed. Because of its larger electrode area for a given cell capacity, the multiplate cell is expected to have a higher utilization of active material than that of the bicell.

The cell shown in Fig. IV-2 is assembled with two uncharged positive electrodes† and three partially charged negative electrodes (typical electrode dimensions, 16.9 × 17.8 cm). The positive electrode consists of a hot-pressed plaque of FeS (uncharged, *i.e.*, Li_2S and Fe) placed on each side of a flat-sheet current collector and is held together by metal frames. The electrode is completely covered by a BN-felt separator/retainer, which is wet with electrolyte. The negative electrode consists of pressed aluminum wire plaques containing a predetermined amount of lithium-aluminum alloy; a metal frame surrounds this electrode. A screen-type current collector is welded to the cell can on assembly. The surface area of the positive electrode is slightly less than that of the negative electrode to allow insulation of the edges of the positive electrode from negative potential. The electrical connection of the positive electrode plates to the feedthrough is made by a strap that is welded to the current collector of both positive electrodes. This strap, which is made of the same material as the current collector, is insulated from the negative plates by a thin bar of boron nitride. The top area of the electrode plates, other than the part insulated by the boron nitride bar, is completely filled with BN powder. The electrical feedthrough for this cell is an ANL snap-ring type (ANL-77-75, p. 32).

---

*Research Student Associate, Institute of Nuclear Energy Research, Taiwan.

†In this cell design, each positive electrode has two facing negative electrodes.

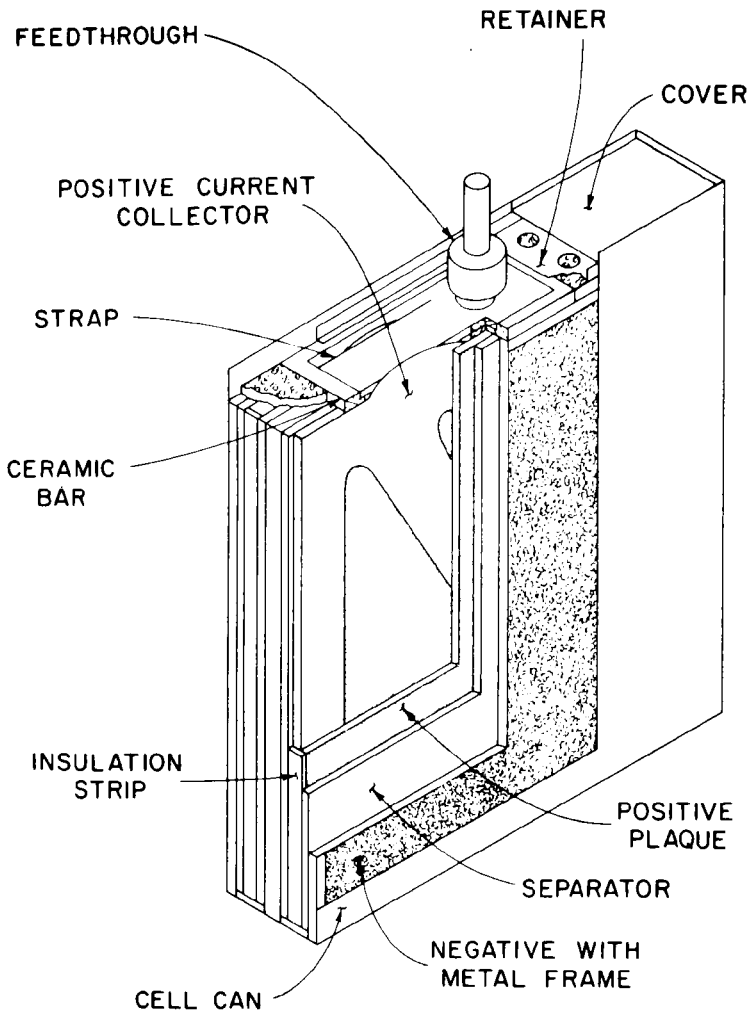

Fig. IV-2. Multiplate Cell Design.

The total weight for the multiplate cell is about 2.55 kg. Calculations indicate that a multiplate cell with this design will achieve an energy of 334 W-hr and a utilization of 75% (theoretical capacity, 278 A-hr) at a current density of 60 mA/cm^2. These figures correspond to a specific energy of 131 W-hr/kg at the 4-hr rate. Table IV-1 presents the projected materials cost for this multiplate cell design. The materials cost is expected to be \$23.2/kW-hr. However, if a MgO-powder separator is used in this cell instead of BN felt, the materials cost would be reduced to \$12.8/kW-hr.

B. Development of MS_2 Cells

Cell chemistry studies (ANL-77-75, pp. 52-53) indicated that NiS_2 is an attractive alternative to FeS_2 as the active material in the positive electrode. Consequently, the recommendation was made that the use of NiS_2 as a substitute for the active material in the positive electrode or as an additive in Li-Al/MS_2 cells be investigated in engineering-scale cells.

Table IV-1. Materials Costs for the ANL Multiplate Cell

	Weight, kg/kW-hr	Projected Cost $/kg	Projected Cost $/kW-hr
Positive Electrode Components			
Li_2S	1.0	3.70	3.70
Fe Powder	1.2	0.20	0.24
LiCl-KCl	0.67	1.20	0.80
Fe (Current Collector)	0.3	0.15	0.05
Negative Electrode Components			
Al	1.7	1.10	1.90
Li	0.07	17.00	1.20
LiCl-KCl	0.67	1.20	0.80
Separator Components			
BN Felt	0.2	57.5	11.50
LiCl-KCl	0.8	1.20	0.90
Other			
Insulation	0.3	1.20	0.40
Feedthrough	0.7	0.45	0.45
Miscellaneous	0.7	--	1.26
TOTAL	8.31		23.2

1. Uncharged MS_2 Cells with Pressed Electrodes
(L. G. Batholme)

An engineering Li-Al/NiS_2-CoS_2 cell, namely, R-31, was assembled in the uncharged state with hot-pressed electrodes. This cell has been operating for more than 221 days and 513 cycles. In this period, the capacity declined less than 20%. In a similar cell, R-36, carbon powder that had been heat-treated at 1000°C was added to the positive electrode to enhance current collection. This cell has operated for over 142 cycles (92 days) and has maintained a lower resistance and higher utilization than R-31.

2. Charged MS_2 Cells with Pressed Electrodes
(F. J. Martino)

An M-series cell, M-4, was built with a positive electrode containing a mixture of iron sulfide and nickel sulfide (69 mol % $FeS_{1.46}$ - 31 mol % $NiS_{1.46}$) as well as molybdenum powder to improve current collection. A lower sulfur-to-metal ratio in this cell was expected to improve cell lifetime over that of previous MS_2 cells. Cell M-4 operated for 300 cycles (172 days) and retained nearly 83% of its initial capacity (112 A-hr at the 4-hr rate). A summary of the cell capacity over the 300 cycles is shown in Fig. IV-3.

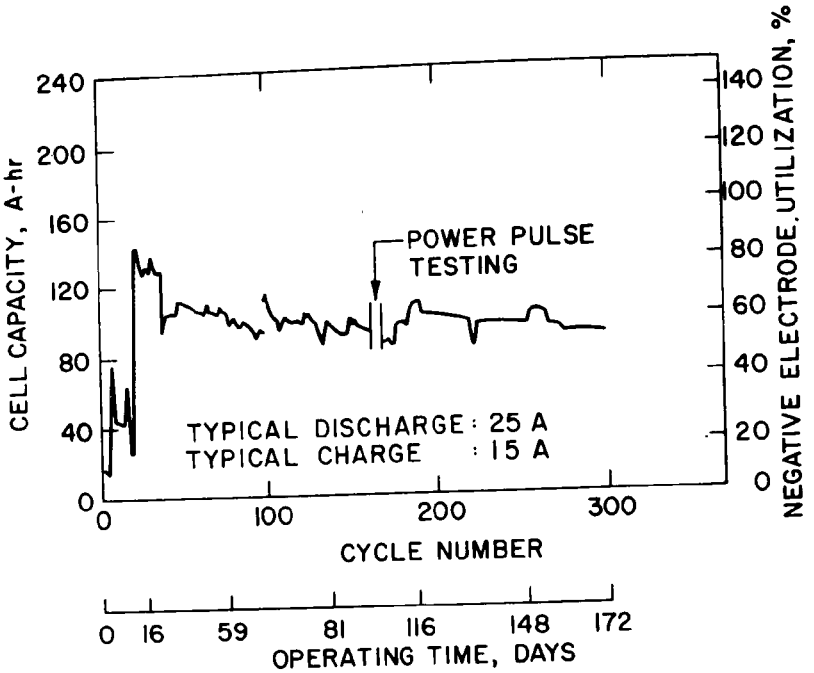

Fig. IV-3. Performance Data on Cell M-4

Another M-series cell, M-7, had a design similar to that of M-4 except for the following features: cell capacity* was limited by the positive electrode, the positive-electrode thickness was 25% less, and the negative electrode had 55 at. % LiAl.† To date, Cell M-4 has operated for 80 cycles (55 days). Performance data on Cells M-7 and M-4 are presented in Table IV-2. As can be seen in this table, the performance of Cell M-7 is better than that of M-4.

Table IV-2. Performance Data on Cells M-4 and M-7

	Capacity,[a] A-hr	Energy,[a] W-hr	Specific Energy,[a] W-hr/kg	Specific Power,[b] W/kg		Cell Resistance, mΩ
				100%	50% Charge	
Cell M-7	103	150	97	200	125	2.4
Cell M-4	107	152	87	145	90	3.2

[a]Measured at 25 A current (4-hr rate for Cell M-7 and 4.5-hr rate for Cell M-4).

[b]15-sec pulse.

*Capacity loading: Cell M-4, 165 A-hr/267 A-hr; Cell M-7, 233 A-hr/194 A-hr.

†Cell M-4 had 48 at. % LiAl.

3. Carbon-Bonded MS_2 Cells
(T. D. Kaun)

a. Cells with FeS_2 Carbon-Bonded Electrodes

The KK-series cell (KK-4, -6, -9, -10, -11) was developed to test FeS_2 cells with carbon-bonded* electrodes. These cells had a compact design, a carbon-bonded positive electrode, a molybdenum current collector, and BN-fabric separators (except Cell KK-11 which had a Y_2O_3-felt separator). Testing of these cells showed that cell resistance is not reduced by increased cell compactness, but by modifications in the current collector design. The effect of modifications in the current collector design on cell resistance is shown in Table IV-3. The cells with the lowest resistance (KK-10, -11) had a vertical terminal rod of molybdenum that extended into the active material and was welded to the molybdenum current collector to form a central bus bar. (This design was used in the M-series cells.) Preliminary studies indicated that further reduction in cell resistance is obtainable by the addition of conductive powders such as carbon or molybdenum to the positive electrode.

An FeS-Cu_2S cell with the KK-series design (KK-5) was built with the same type of current collector as that of Cell KK-11; however, the current collector of Cell KK-5 was made of iron, not molybdenum. During operation, this cell maintained very low resistances (3.8 mΩ).

Table IV-3. Resistances of KK-series Cells

Date of Operation	Cell No.	Typical Cell Resistance	Positive-Electrode Current Collector Design
1/76	KK-4	5.5 mΩ	Split Mo rod inserted into 1/2 electrode depth and riveted to current collector.
7/76	KK-6	7.0 mΩ	Horizontal bus bars of nickel welded to top of Mo sheet.
1/77	KK-9	9-10 mΩ	Tab, riveted and spot welded to the honeycomb current collector of Mo.
3/77	KK-10	4.5 mΩ	Quartered Mo rod inserted into 1/2 electrode depth and welded to current collector.
4/77	KK-11	3.6 mΩ	Quartered Mo rod (with machined tolerance) inserted into 4/5 electrode depth and welded to current collector.

*For a detailed description of the carbon-bonding technique see ANL-77-18, p. 15.

b. Cells with NiS_2 Carbon-Bonded Electrodes

Cell KK-13, which has a carbon-bonded positive electrode of NiS_2-CoS_2 and a Y_2O_3-felt separator, has operated for 310 cycles (170 days). After 200 cycles of operation, the coulombic efficiency of this cell dropped from 99.5 to 90%. This drop in efficiency is typical of cells using Y_2O_3-felt separators. At cycle 290 the cell was accidentally overcharged due to a voltage-lead problem. This overcharge resulted in a coulombic efficiency of 70%. For the last 175 cycles, the charging rate was increased from 8 to 4 hr, which instead of reducing cell capacity as is typical of FeS_2 cells, increased the NiS_2 cell capacity. Since the performance of this cell is affected by changes in temperature (ANL-78-21, p. 36), it was concluded that the higher charging rates produce localized heating which speeds up the electrode kinetics. During the lifetime of Cell KK-13, the capacity declined by less than 16% of its initial value (100 A-hr at the 4-hr rate).

c. Development of Cells with Powder Separators
(T. W. Olszanski)

The operation of three engineering-scale FeS cells containing MgO-powder separators, namely, PW-8, -9, and -10, is continuing (see ANL-78-21, p. 38). The separator of Cell PW-9 was hot-pressed onto both sides of the positive electrode and then loaded into the cell. The separators of Cells PW-8 and -10 were loaded into the cell by a vibratory technique. Unlike the designs of PW-8 and PW-9, the design of Cell PW-10 was optimized for specific energy and internal resistance (a thinner separator and positive terminal rod).

These three cells have operated for the following periods: Cell PW-8, 408 cycles (171 days); Cell PW-9, 130 cycles (65 days); and Cell PW-10, 104 cycles (63 days). All three cells have maintained coulombic efficiencies over 98%. The internal resistances of Cells PW-8 and PW-9 have averaged about 8-10 mΩ. The utilization of Cell PW-9 (42% at a current density of 34 mA/cm^2) was 5% greater than that of Cell PW-8. The cell capacity and coulombic efficiency of Cell PW-9 are shown in Fig. IV-4. Cell PW-10, which was optimized for performance and operated at 500°C, achieved a specific energy of 60 W-hr/kg at the 5-hr rate and maintained an internal resistance of 6 mΩ.

A small-scale FeS cell with a calcium sulfide powder separator has operated for over 414 cycles (146 days). Its coulombic efficiency averaged >98% throughout cell operation.

Thus far the cells using powder separators have proven capable of producing consistently high coulombic and energy efficiencies. The chemical stability, low cost, and ease of assembly of the powder separator makes it a potentially attractive separator material.

d. Cell Assembly in Air
(C. C. Hsiang,* L. G. Batholme)

An effort to fabricate a Li-Al/FeS_x cell in air rather than in a helium atmosphere is under way. Sensitivity of the X-phase material (Li_2FeS_2) to air has been determined by measuring weight increases of this

*Research Student Associate, Institute of Nuclear Energy Research, Taiwan.

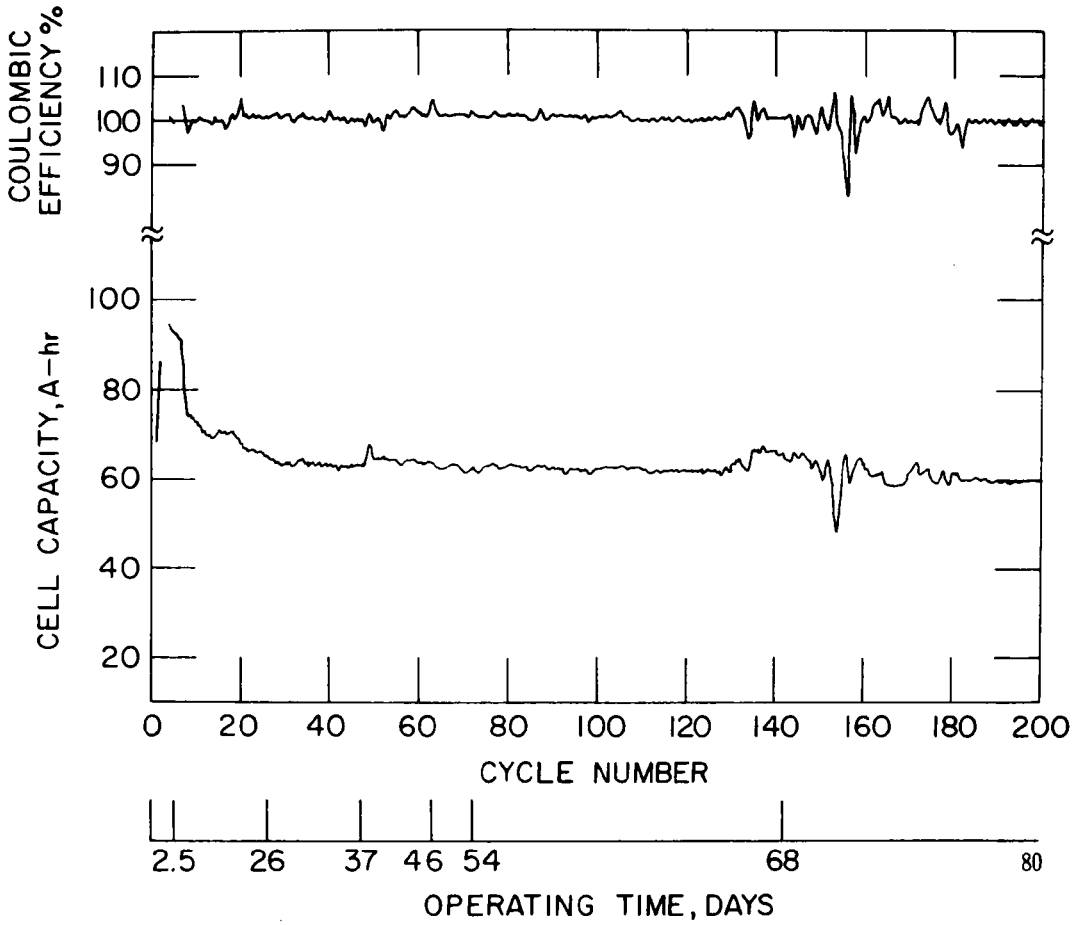

Fig. IV-4. Performance Data on Cell PW-9

material in air. The results have shown that a powder form of the X-phase material can be handled in air for up to six hours with no changes in weight. An X-ray diffraction analysis showed minor hydrate formation after 24 hours of exposure to air. An engineering cell is now under construction to test the performance of a cell assembled in air.

V. MATERIALS DEVELOPMENT
(J. E. Battles)

Efforts in the materials program are directed toward the development of various cell components (electrode separators, current collectors, and cell hardware), testing and evaluation of cell materials (corrosion and wettability testing), and post-test examinations of cells to evaluate the behavior of the electrode and construction materials.

A. Electrode Separator Development
(R. B. Swaroop and C. W. Boquist)

Felt, powder, and paper separators are being developed as alternatives to the BN fabric currently used in Li-Al/FeS cells. These candidate separators will be less expensive and technically superior to the BN fabric.

1. In-Cell Testing

A Li-Al/FeS cell, SC-25 (separator-test cell design*), with a separator of 1.25-mm thick BN felt, was put into operation. After a degassing operation at the end of the 96th cycle, the cell performance, which had been exceptional up to this point, declined sharply and the cell could not be recharged. On post-test examination fine iron particles from the positive electrode were found in the separator; this particle movement was apparently caused by the degassing of the cell. Another Li-Al/FeS cell, SC-27, was constructed with a separator of BN felt that had been treated with $LiAlCl_4$ powder prior to cell assembly.† The initial utilization of this cell was approximately the same as that of SC-25 ($\sim$60% at 40 mA/cm^2).

2. Out-of-Cell Testing

A recently received batch of BN felts from Carborundum Co. was characterized. The as-received felt ranged from 21 to 22 mg/cm^2 in linear density, 5.5 to 9.5 kPa in burst strength, 90 to 93% in porosity, and 1.1 to 1.5 mm in thickness. After stabilization of this felt in nitrogen at 1750°C, the porosity and thickness remained about the same and the linear density and burst strength decreased slightly. In additional studies, the bonding structure of these felts was examined both before and after stabilization; stabilization did not affect the bonding structure. The Carborundum felt was easy to handle in subsequent cell construction.

Flow-behavior studies with two pellets (50% porous) of FeS powder and LiCl-KCl eutectic were continued. The objective of these experiments is to determine the minimum stress level required to initiate flow in an FeS electrode. The experiment was done in a manner similar to that described previously (ANL-78-21, p. 41) except that once 450°C was reached the pressure on the specimen, previously held constant at 55 kPa (8 psi), was gradually increased while the temperature was held constant. One of the FeS plus salt pellets was placed in a quartz crucible, which constrained all the surfaces of the specimen except the top (where the stress was applied).

---

*See ANL-77-75, p. 34 for the general design of the separator-test cell.

†In ANL-78-21, p. 48 this powder was found to improve the wettability of the separator by molten electrolyte.

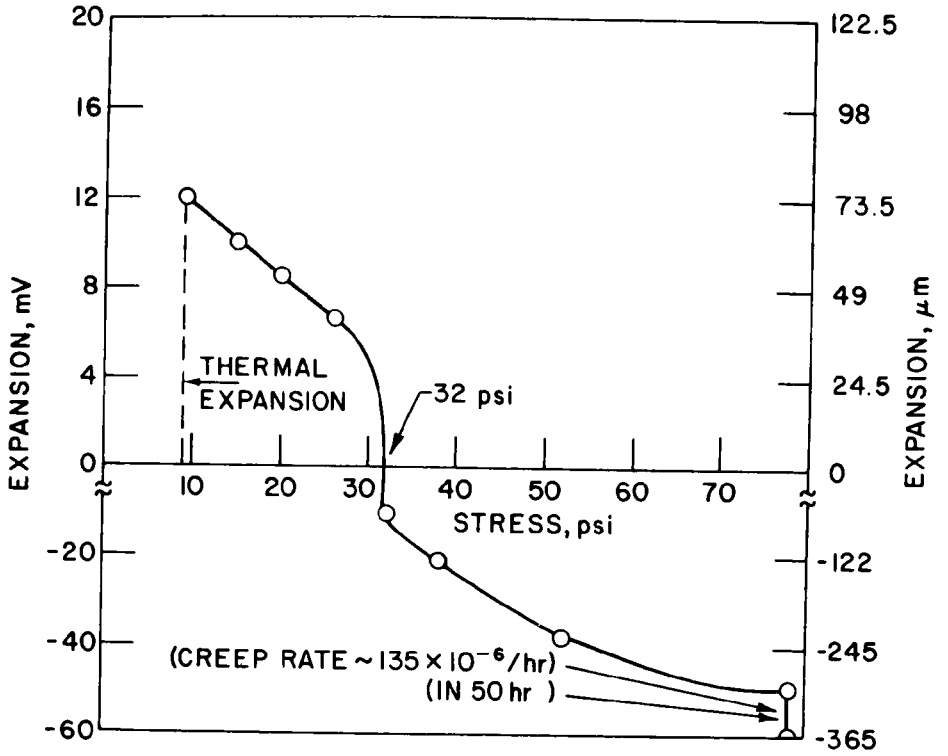

Fig. V-1. Creep Behavior of FeS + LiCl - KCl Sample (Constrained) at 450°C.

Figure V-1 shows the deformation of the unconstrained specimen as a function of pressure at 450°C. As can be easily seen in this figure, the FeS material flows significantly at stress levels of 210 to 245 kPa (30-35 psi). This flow is continuous and occurs in the upward direction (normal to the one unconstrained surface) relative to the specimen. Between room temperature and 450°C, the measured thermal expansion coefficient is 15×10^{-6}/°C under a stress of 55 kPa (8 psi); at 450°C the creep rate is 135×10^{-6} m/m per hour under a stress of 546 kPa (78 psi). The unconstrained FeS plus salt specimen also showed significant flow at stress levels of 210 to 245 kPa, and the direction of the flow was normal to the applied load (*i.e.*, along the transverse surfaces). This behavior is consistent with the observed tendency of inadequately constrained electrodes to extrude material.

The above experiment indicates that FeS electrode material, when under stresses of ∿210 kPa, may extrude into the empty spaces in the cell. However, extrusion of active material is also dependent on the particle size of the FeS and salt.[5,6]

B. Ceramic Materials Development

(G. Bandyopadhyay, J. T. Dusek, and T. M. Galvin)*

This effort is concerned with the development of rigid, porous separators and electrically conductive ceramic-coated current collectors. Additional effort was devoted to the completion of a dry box with six furnace wells that will be used for in-cell testing of the rigid, porous separators.

---

* Materials Science Division, ANL.

A number of different processing techniques have been attempted for the fabrication of porous Y_2O_3 separators. In one of these techniques, various compositions of Y_2O_3 powder and nitric acid were cast into plaster plates (see ANL-78-21, p. 43). This technique appears to be particularly promising because the Y_2O_3-nitric acid plaster sets by a nucleation and growth mechanism which results in a uniform microstructure. However, warpage during the sintering of the Y_2O_3-nitric acid plaster is a problem. Additional experiments were performed to characterize Y_2O_3-nitric acid plaster and to determine processes that would eliminate warpage during sintering.

The Y_2O_3-nitric acid plaster was characterized by scanning-electron microscopy and X-ray diffraction analysis.* As reported earlier (ANL-77-17, p. 35), the microstructure consisted of a mass of tangled needle and plate-like crystals with random orientation and a continuously connected network of small pores. The X-ray diffraction analysis indicated the presence of unidentified phases in addition to some unreacted Y_2O_3. The unidentified phase is assumed to be hydrated Y_2O_3 ($Y_2O_3 \cdot xH_2O$) which sets as a plaster. X-ray diffraction has also established that Y_2O_3 plaster easily converts to Y_2O_3 during calcination or sintering at high temperature (>1200°C). The following processes to eliminate warpage during sintering have been investigated: (1) the set plaster was crushed, screened, cold pressed, and sintered at various temperatures, and (2) the set plaster was calcined at 1250°C for 8 hr and then crushed, screened, cold pressed, and sintered at various temperatures. Both processes resulted in a significant reduction of warpage in the fired separator plates ($\sim$80 × 60 × 2.5 mm). Density data for a number of discs and plates prepared by the above procedures are listed in Table V-1. As can be deduced from this table, the plates prepared from crushed plaster resulted in significantly lower densities than those obtained from calcined Y_2O_3 plaster or from the as-received Y_2O_3 powders.† The calcined plaster samples had very little shrinkage during sintering.

The sintered samples prepared from crushed plaster, calcined plaster, and as-received Y_2O_3 were examined by scanning-electron microscopy. In all cases, the microstructures were characterized by agglomerates of small crystallites with larger pores ($\sim$5 μm) between the agglomerate particles (see Fig. V-2). Preliminary in-cell tests with these separators will be conducted during the next quarter.

In addition to the work on Y_2O_3 separators, preliminary studies have begun on the fabrication of rigid, porous MgO separators by cold pressing and sintering.

A dry box with six furnace wells has been assembled. The box has an argon atmosphere with less than 10 ppm moisture. Furnace thermocouples have been calibrated, and preliminary tests on the static corrosion behavior of porous Y_2O_3 samples have begun. Minicyclers, electronic equipment, and cell hardware components are expected to be available soon.

---

*Performed by B. S. Tani, Analytical Chemistry Laboratory, ANL.

†Manufactured by Molycorp. Inc., White Plains, NY (99.99% Y_2O_3).

Table V-1. Density Data for Various Sintered Y_2O_3 Specimens

Composition	Sample Geometry[a]	Sintering Temp, °C	Sintering Time, hr	Fired Density, % of Theor.
Crushed Y_2O_3-Nitric Acid Plaster	Disc	1400	None	38.8
	Plate	1425	None	39.2
	Plate	1500	None	42.2
	Disc	1500	2.0	44.7
Calcined Y_2O_3-Nitric Acid Plaster	Disc	1400	None	46.0
	Plate	1425	None	45.2
	Plate	1500	None	51.8
	Disc	1500	2.0	48.1
Y_2O_3Powder	Disc	1400	None	49.0

[a]Dimensions of unfired discs: 32-mm dia, ∿2.5-mm thickness; dimensions of unfired plates: 113 × 82 × ∿3 mm.

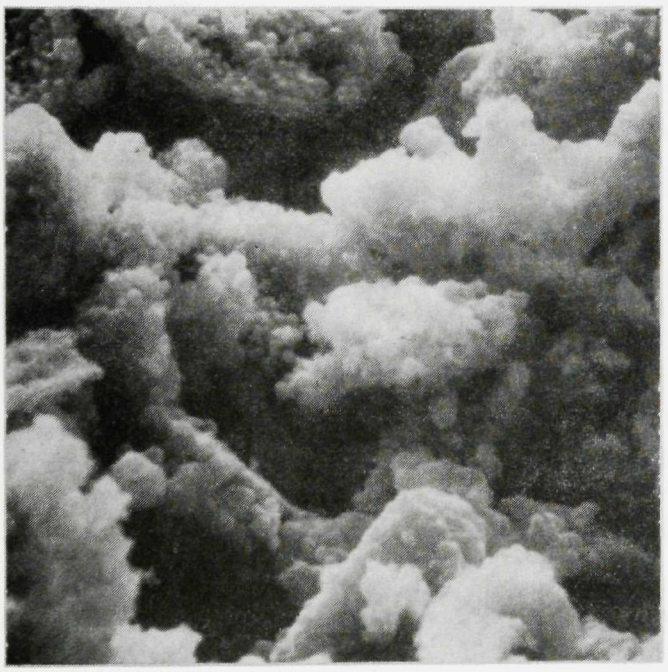

Fig. V-2. Microstructure of a Y_2O_3 Sample Prepared from Crushed Y_2O_3-Nitric Acid Plaster (cold pressed and sintered at 1400°C with no hold time; density 38.8% TD; magnification, 8000 X.

Last quarter, three candidate coating materials for use with inexpensive positive-electrode current collectors were identified--titanium nitride, titanium boride, and iron boride. A number of outside vendors have been contracted to coat AISI 1008 steel substrates with these ceramics. Steel substrates (0.457- and 0.635-mm thick) are being fabricated at this time and will soon be sent to the vendors. The microstructure of these coated samples will be examined, and the samples will undergo thermal-shock and corrosion tests.

C. Cell Wetting and Degassing Studies
(J. G. Eberhart)

During this quarter experiments were continued to identify the factors that influence cell material wettability and to explore possible means of altering undesirable wetting behavior.

In previous experiments (ANL-77-75, p. 42) we wetted BN samples (both fabric and felt) with molten LiCl-KCl by the following technique. The BN samples were completely immersed in molten LiCl-KCl contained in a helium-atmosphere furnace well, and then the furnace well was evacuated and repressurized with helium. Although completely wetted by the salt, samples prepared by this method were too warped for use in cells. Therefore, we repeated the above procedure with both sides of the BN material completely covered by metal plates to prevent warping. After repressurization of the furnace well with helium, the BN felt was infiltrated by the molten salt (through the exposed felt edges) but the BN fabric was not. Unfortunately, wetted felt that was large enough for use in engineering cells cracked when cooled. Nonetheless, the above results indicate that, during start-up, a cell with BN felt separators should wet more readily than a cell with BN fabric separators.

Two ANL cells, namely, M-7 (see Section IV) and SC-26 (a separator-test cell) employed one or more photo-etched, stainless steel screens as particle retainers. Both cells displayed a very high initial internal resistance which appeared to be associated with difficulty in wetting this new particle retainer with molten electrolyte. Electrolyte penetration and contact angle measurements made on the screen suggested that this wetting problem was caused by the sharp corners at the top and bottom of each photo-etched hole. Sharp corners are generally known to act as a barrier to advancing liquids. Treatment of the screen with molten $LiAlCl_4$ at 200°C improved the wettability of the screen; and, subsequently, the photo-etched holes were spontaneously penetrated by molten LiCl-KCl.

Electrolyte penetration tests were performed on rigid, porous Y_2O_3 specimens. Four specimens of varying porosity and fabrication procedures were examined. Only one of the four specimens was spontaneously penetrated by molten LiCl-KCl. The reasons for the differences observed in penetration behavior of these Y_2O_3 samples are not presently understood.

Measurements of advancing (θ_A) and receding (θ_R) contact angles have been continued (see ANL-78-21, p. 47) for molten electrolyte on various cell materials. The following observations have been made: electrolyte spreads ($\theta_R = \theta_A = 0$) on Li-Al alloy; Type 304 stainless steel and yttria are easy to

wet ($\theta_R < \theta_A < 90°$); and FeS_2, FeS, Li_2S, Fe, Al, BN, MgO, and ZrO_2 are difficult to wet ($\theta_R < 90° < \theta_A$). Electrolyte spontaneously penetrates the pore structure of an easy-to wet cell component, but must be forced into the pores of a difficult-to-wet component.

A knowledge of receding contact angles for cell materials permits the estimation of the height to which a porous battery material can maintain electrolyte infiltration. The receding capillary height was calculated with the aid of a conservative model[7] for the porous cell material; this model assumes a cubic packing of uniform, sperical particles. For the cell material with poorest wetting characteristics (Li_2S), particle sizes of 1000, 100, and 10 μm yield receding capillary heights of 3.5, 35, and 350 cm, respectively. Since a height of 35 cm is adequate for any foreseeable engineering cell, a particle size of 100 μm or less is recommended for powder-formed cell components on the basis of simple capillarity considerations.

The degassing and attendant pressure build-up which can occur during the operation of a cell is probably detrimental to its efficiency and lifetime. Thus, a study has been under way to characterize, by mass spectrometry, the gaseous species produced while cells are in a charge, discharge, or open-circuit mode. The quadrupole mass spectrometer, which was sent to Varian Associates, Inc. for repairs and calibration, has been returned to ANL. The instrument has been reassembled and its operation is presently being tested.

D. Corrosion Studies
(J. A. Smaga)

Current collectors in the positive electrode are exposed to a corrosive environment consisting of one or more metal sulfides and molten electrolyte. A previous series of static corrosion tests examined the corrosion rate of representative current collector materials in equal-volume mixtures of LiCl-KCl and FeS, FeS_2, CoS_2, or Cu_2S at 450°C (ANL-77-68, p. 40). A second series of tests has been completed in which the corrosiveness of NiS, NiS_2, $CuFeS_2$, and TiS_2 were similarly tested. These tests were conducted at 450°C for periods as long as 1000 hr, and the results are summarized in Table V-2.

As can be seen in Table V-2, the sulfide environments for any given current-collector material are listed in order of increasing corrosiveness, with one exception (the corrosion rate of Type 304 SS is less in $CuFeS_2$ than in NiS). By combining the results in this table with the results of our previous studies (ANL-77-68, p. 40) we deduced that the corrosiveness of the metal-sulfide environments increases in the following order: FeS, Cu_2S, $CuFeS_2$, NiS, FeS_2, TiS_2, NiS_2, CoS_2. The corrosion rates for all of the current-collector materials were two or three orders of magnitude higher in the NiS and $CuFeS_2$ environments than in the FeS environment. The corrosion rates for all of the current collector materials were higher in the NiS_2 and TiS_2 environments than in the FeS_2 environment, although the differences in corrosion rates were never more than a factor of two. This result indicates that an alloy material probably should not be used in FeS_2 cells. Molybdenum had excellent corrosion resistance in the TiS_2 and NiS_2 environments as well as in the FeS_2.

Table V-2. Corrosion Rates for Selected Metals Tested at 450°C in Equal-Volume Mixtures of Metal Sulfides and Electrolyte

Material	Sulfide Environment	Average Corrosion Rate, μm/yr[a]	Remarks and Reaction Products[b]
AISI 1008	$CuFeS_2$	>5000	Complete reaction in 500 hr.
	NiS	>5000	Complete reaction in 500 hr.
Type 304 SS	$CuFeS_2$	4500	Severe intergranular attack.
	NiS	2200	Intergranular attack.
	TiS_2	>6300	Complete reaction in 500 hr.
	NiS_2	>6300	Complete reaction in 500 hr.
Nickel	$CuFeS_2$	1600	Localized intergranular attack.
	NiS	2400	Uniform surface attack.
	TiS_2	3200	Open, detailed scale structure; Ni_3S_2.
	NiS_2	>6000	Compact, monolithic scale; NiS, NiS_2.
Inconel 625	$CuFeS_2$	430	Surface depletion zone.
	NiS	490	General surface attack.
	TiS_2	1700	Intergranular attack.
	NiS_2	1900	Complex scale structure; NiS, NiS_2.
Hastelloy B	$CuFeS_2$	98	Minor surface depletion zone.
	NiS	120	Moderate surface attack.
	TiS_2	650	General surface attack; $NiS_{1.03}$.
	NiS_2	530	Surface depletion zone.
Molybdenum	TiS_2	+0.2	No apparent attack.
	NiS_2	+5.5	Probably MoS_2 layer.

[a]Each corrosion rate is the average value for 500- and 1000-hr tests. Values preceded by "+" represent the rate of formation for an adherent reaction layer; these preceded by ">" represent the minimum corrosion rate based on initial sample thickness.

[b]X-ray diffraction analyses to determine reaction products were conducted by B. S. Tani, Analytical Chemistry Group, ANL.

E. Post-Test Cell Examinations

(F. C. Mrazek, N. C. Otto, and J. E. Battles)

Post-test examinations are conducted on small laboratory cells* and on engineering-scale cells.† The objectives of these examinations are to determine (1) cell morphology (such as electrode microstructure, active material distribution and utilization, reaction uniformity, components' performance, impurities, and cross-contamination of electrodes), (2) in-cell corrosion

*Fabricated and tested at ANL.

†Fabricated either at ANL or an industrial firm and tested at ANL.

reactions and kinetics, and (3) causes of cell failure. These results are evaluated, and appropriate recommendations for improving cell performance and lifetime are made.

1. Causes of Cell Failure

During this report period, a total of 16 vertical, prismatic engineering cells were examined. Twelve cells had failed because of short circuits, and one because of a significant loss in capacity. Operation of three cells was ended because the cell testing period was completed (no failure). The results of the post-test cell examinations are listed in Table V-3. Three cells are of particular interest--M-6, EP-I-8-C-10, EP-I-7-1.

In Cell M-6, a significant loss of capacity occurred after the cell had been operated at 500°C for a short period of time and returned to the normal operating temperature (450°C). The resistance of the cell at ambient temperature was >3 MΩ which is greater than that of any previous cell. Metallographic examinations indicated morphologies typical for the negative and positive electrodes of FeS-Cu_2S cells. Corrosion of the current collectors was excessive but is attributable to cell operation at 500°C. A possible cause of the capacity loss in this cell is that a thin film may have formed on the negative electrode materials and hindered the cell reaction. Additional examinations are being conducted.

The cause of failure in Cell EP-I-8-C-10 was attributed to the heavy concentration of Li_2S(Fe)* and Li_2FeS_2 in the BN-felt separator. In all previous post-test examinations of FeS_2 cells, a band of Li_2S(Fe) has been found in the separator (parallel to the electrode face). Because of the thinness of the felt separator in this cell (<1.5 mm), the Li_2S(Fe) deposit extended across the separator thickness in some areas, thereby causing a short circuit. This result indicates that a thin separator of BN felt is not adequate for FeS_2 cells because of the formation of Li_2S(Fe) deposits in the separator.

The short circuit in Cell EP-I-7-1 was caused by extensive metallic iron deposits across the separator. This behavior has been previously observed in overcharged FeS cells. Also, the Li_2S(Fe) band normally found in the separators of FeS_2 cells was absent. These observations, combined with the lack of the upper plateau in the voltage curves (typical of FeS_2 cells), indicate that FeS rather than FeS_2 was used in this cell.

A summary of cell failure mechanisms for cells examined during this report period is listed in Table V-4, which also presents the cell failure mechanisms for the 97 cells examined to date. During this period, four cases of failure from improper cell assembly were identified, thus indicating a need for closer quality control in cell assembly. In addition, three cases of separators cut by the honeycomb current collectors were identified; however, these cells were fabricated prior to the recommendation to add protective screens. The causes of failure could not be identified in 15% of the total cells examined to date. Most cell failures have been mechanical in origin, as shown in Table V-4. Corrective actions have been recommended and are being incorporated in the recent cells with the expectation that the major causes of failure will be eliminated.

*This compound consists of Li_2S and Fe particles.

Table V-3. Results of Post-test Cell Examinations

Cell Number And Type	Cell Lifetime Days	Cell Lifetime Cycles	Reason Terminated	Date Examined	Cause of Failure
EP-I-8-A-1 Li-Al/FeS_2-CoS_2	31	33	Short circuit	1/10/78	The as-received cell resistance was 13 Ω. No evidence of an internal short circuit. The probable cause of low resistance was the Li_2S, X phase, and Z phase observed in the separator.
EP-I-8-A-2 Li-Al/FeS_2-CoS_2	8	5	Short circuit	1/10/78	The as-received cell resistance was 3 Ω. No evidence of an internal short circuit identified. Li_2S and X phase observed in the separator.
EP-I-8-C-9 Li-Al/FeS_2-CoS_2	4	3	Short circuit	1/10/78	The as-received cell resistance was 0 Ω. The short circuit was caused by a band of very fine metallic particles across the separator thickness.
EP-I-8-D-13 Li-Al/FeS_2-CoS_2	55	72	Short circuit	2/3/78	Short circuit caused by the honeycomb current collector cutting through the separator.
EP-I-8-F-17 Li-Al/FeS_2-CoS_2	63	251	End of test	2/3/78	The as-received cell resistance was 2.1 kΩ.
EP-I-8-G-19 Li-Al/FeS_2-CoS_2	31	86	End of test	2/3/78	The as-received cell resistance was 390 Ω.
EP-I-5-5 Li-Al/FeS_2-CoS_2	227	267	Short circuit	3/15/78	Short circuit caused by honeycomb current collector cutting through the separator.
EP-I-8-B-5 Li-Al/FeS_2-CoS_2	45	53	Short circuit	3/15/78	Short circuit caused by expansion of positive electrode material that ruptured the BN felt separators and the negative electrode screen.

Table V-3. (contd)

Cell Number And Type	Cell Lifetime Days	Cell Lifetime Cycles	Reason Terminated	Date Examined	Cause of Failure
EP-I-8-C-10 Li-Al/FeS_2-CoS_2	23	18	Short circuit	3/15/78	Short circuit caused by the heavy concentration of Li_2S and Li_2FeS_2 in the BN felt separator, which formed a complete bridge between the elctrodes.
EP-I-8-E-15 Li-Al/FeS_2-CoS_2	8	11	Short circuit	3/15/78	Short circuit caused by the honeycomb current collector cutting through the separator.
EP-I-7-1 Li-Al/FeS_2-CoS_2	66	118	Short circuit	3/17/78	Short circuit apparently caused by overcharge that deposited large amounts of metallic iron throughout most of the separator thickness.
R-32 (U)[a] Li-Al/NiS_2+C	94	178	Short circuit	1/20/78	Short circuit caused by extrusion of positive electrode material through an opening in the BN fabric separator.
R-33 (U) Li-Al/FeS_2-NiS_2+C	69	118	Short circuit	1/20/78	Short circuit caused by extrusion of positive electrode material through an opening in BN fabric separator.
R-34 (U) Li-Al/FeS-Cu_2S+C	68	144	Short circuit	2/17/78	Short circuit caused by the ZrO_2 cloth of the positive electrode contacting the negative electrode frame.

(contd)

Table V-3. (contd)

Cell Number And Type	Cell Lifetime Days	Cell Lifetime Cycles	Reason Terminated	Date Examined	Cause of Failure
R-35 (U) Li-Al/$FeS_{1.75}$+Co+C	43	50	Short circuit	2/17/78	Short circuit caused by the extrusion of the positive electrode material through a rupture in the retainer screen and BN fabric adjacent to the Hastelloy B frame. This rupture was probably caused by swelling of the positive electrode.
M-6 Li-Al/FeS-Cu_2S+C	44	64	Loss of Capacity	3/2/78	As-received cell resistance was >3 MΩ. No short circuit; loss of capacity occurred after operation at 500°C. The cause of failure was not identified. Corrosion was more extensive than normal.

[a]The symbol U indicates cell assembled uncharged.

Table V-4. Causes of Cell Failure

	Cases[a]	
	This Period	Overall
Extrusion of active material	2	22
Metallic Cu in separator[b]	0	11
Separator cut by honeycomb current collector	3	20
Equipment malfunction[c]	0	7
Short in feedthrough	0	4
Improper cell assembly	4	9
Broken positive conductor	0	2
Metallic and/or sulfide deposits across separator	2	2
Unidentified		
Declining coulombic efficiency	0	10
Short circuit	1	5
Loss of capacity	1	1

[a]This includes all vertical, prismatic cells that have undergone post-test examinations to date.

[b]FeS cells only.

[c]Overcharge, temperature excursion, or polarity reversal.

2. In-cell Corrosion Results

In-cell corrosion data on the electrode current collectors have been obtained from the metallographic examinations of both positive and negative electrodes. Plots of the data can be used to predict the expected lifetimes of the current collectors in engineering-scale cells.

In the negative electrode, the current collector material is AISI-1008 low-carbon steel, which reacts with aluminum (lithium depleted Li-Al) to form the brittle intermetallic compound $FeAl_2$. A plot of corrosion penetration *vs.* the square root of time yielded a straight line, thus indicating that the Fe-Al reaction is diffusion controlled. In Fig. V-3, the corrosion penetration of low-carbon steel (125-μm thick) in a negative electrode is plotted as a function of time. The solid line in this figure is based on data from post-test examinations; the dotted line is a projection from this post-test data. As can be seen in this figure, the corrosion penetration of the steel current collector by the negative electrode is projected to be ∿60 μm at 800 days (2.5 years).

The molybdenum current collectors used in the positive electrode of FeS_2 cells react with sulfur to form a thin, adherent layer of MoS_2. As shown in Fig. V-4, the rate of this reaction is exceedingly low. After 900 days of operation, the depth of MoS_2 penetration is projected to be less than 5 μm.

As yet insufficient data has been obtained for a similar treatment of the iron current collector in the positive electrode of an FeS cell.

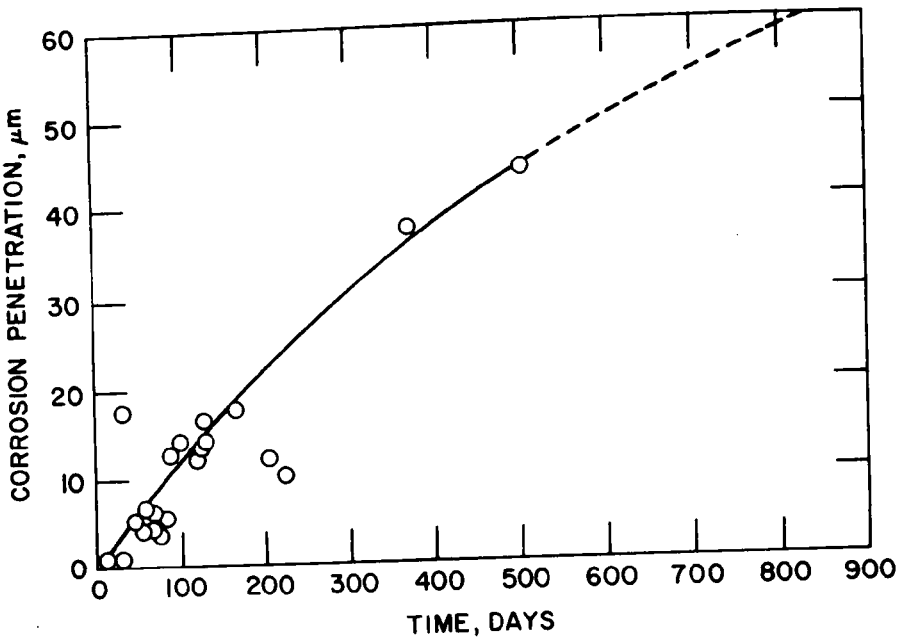

Fig. V-3. Corrosion of Low-Carbon-Steel Current Collector by the Negative Electrode ($Fe + 2Al \rightarrow FeAl_2$)

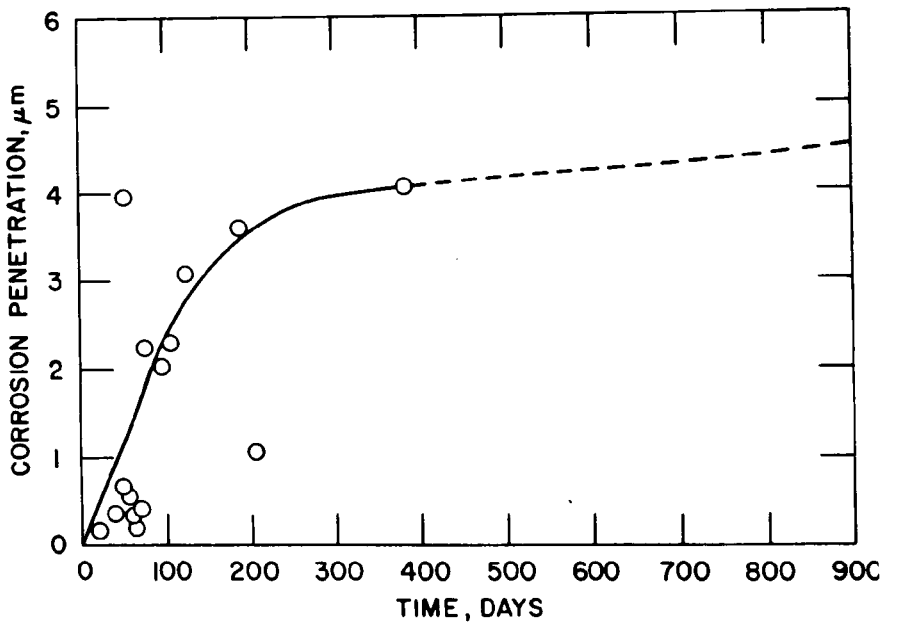

Fig. V-4. Corrosion of Molybdenum Current Collector in the Positive Electrode ($Mo + 2S \rightarrow MoS_2$)

VI. CELL CHEMISTRY
(M. F. Roche)

The objectives of the cell chemistry studies are: (1) to provide solutions for specific chemical and electrochemical problems that arise in the development of cells and batteries, (2) to develop improved compositions for electrodes and electrolytes, and (3) to acquire a basic understanding of the chemistry and electrochemistry of the cells.

A. Chemical Conditions for the Formation of J Phase
(A. E. Martin)

Previous cell chemistry studies (ANL-77-17, p. 45) indicated that the formation of J phase ($LiK_6Fe_{24}S_{26}Cl$) in FeS electrodes has an adverse effect on electrode kinetics. Therefore, we are searching for methods of eliminating or minimizing the effects of J phase formation.

In the absence of J phase, the phases of an FeS electrode* consist of (1) mixtures of Li_2S, Li_2FeS_2, and Fe during the first half of charge (or conversely the second half of discharge) and (2) mixtures of FeS, Li_2FeS_2, and Fe during the second half of charge (or conversely the first half of discharge). The two mixtures probably react with electrolyte to form J phase according to the following reactions:

(first mixture) $6KCl + Fe + 23Li_2FeS_2 \rightarrow J + 5LiCl + 20Li_2S$ (1)

(second mixture) $6KCl + Fe + 20FeS + 3Li_2FeS_2 \rightarrow J + 5LiCl$ (2)

Preliminary tests indicated that these two reactions strongly depend on temperature and electrolyte composition (ANL-77-17, p. 42 and Ref. 8). Thus we decided to determine the maximum temperature at which J phase forms in mixtures 1 or 2 and electrolytes of various compositions. In the experiment, a mixture of Li_2S, Li_2FeS_2 and Fe was heated for 16 hr at a constant temperature in one of the following electrolytes: 58 mol % LiCl-42 mol % KCL (eutectic), 49 mol % LiCl-36 mol % KCl-15 mol % NaCl, the LiCl-KCl eutectic saturated with LiCl, and the LiCl-KCl-NaCl electrolyte saturated with LiCl. After heating, the reaction products were metallographically examined to determine whether J phase had formed. If J phase had formed, then the temperature was slightly increased; if J phase had not formed, then the temperature was slightly decreased. Eventually, these tests defined a temperature, T, at which J phase formed and a slightly higher temperature at which J phase did not form ($T + \Delta T$). The maximum temperature of J phase formation, T_{max} was thus defined as $(T + \Delta T/2) \pm \Delta T/2$.

The results, given in Table VI-1, show that the addition of LiCl significantly decreased T_{max}. With mixture 2, for example, T_{max} was 623°C with LiCl-KCl eutectic, but only 481°C with the eutectic electrolyte saturated with LiCl. Thus, use of a LiCl-rich electrolyte in FeS cells should result in substantial improvements in performance. Additions of NaCl to LiCl-KCl

*A phase diagram of the Li-Fe-S system is given in ANL-78-21, p. 52.

Table VI-1. Maximum Temperature for Formation of J Phase in FeS Electrodes

Electrolyte	T_{max}, °C	
	Mixture (1)[a]	Mixture (2)[b]
58 mol % LiCl-42 mol % KCl (eutectic)	455 ± 4	623 ± 7
49 mol % LiCl-36 mol % KCl-15 mol % NaCl	435 ± 5	623 ± 7
LiCl-KCl eutectic saturated with LiCl	419 ± 2	481 ± 5
LiCl-KCl-NaCl saturated with LiCl	413 ± 5	477 ± 9

[a]Mixture of Li_2S, Li_2FeS_2, and Fe with electrolyte.

[b]Mixture of FeS, Li_2FeS_2, and Fe with electrolyte.

eutectic caused only slight decreases (20°C) in T_{max} for mixture 1 and no decrease in T_{max} for mixture 2.

Reactions (1) and (2) are both important in FeS electrodes, but only reaction (1) can lead to J phase in stoichiometric FeS_2 electrodes (see Li-Fe-S phase diagram, ANL-78-21, p. 52). The temperatures for suppressing J phase formation via reaction (1) are quite low, as can be seen by examining the first column of Table VI-1. This explains why J phase is less of a problem in FeS_2 electrodes than in FeS electrodes.

Additional tests were conducted to check the reversibility of reactions (1) and (2) in eutectic electrolyte. First, J phase was formed by heating mixture 1 and eutectic electrolyte at 445°C and mixture 2 and eutectic electrolyte at 600°C. Portions of these samples were then reheated for 41 to 88 hr and a similar procedure to that described above was done to determine the temperature at which J phase decomposes. These tests showed that J phase decomposed at 465 ± 7°C in the reheated mixture 1 and at 624 ± 4°C in the reheated mixture 2. The good agreement between these temperatures and those in the first row of Table VI-1 demonstrated the reversibility of reactions (1) and (2). Thermodynamic calculations of the relative stabilities of Li_2FeS_2 and J phase are now in progress.

B. Effects of Electrolyte Composition and Cell Temperature on FeS Cell Performance

(Ching-Kai Ho,* K. E. Anderson,† D. R. Vissers)

A study of the effects of electrolyte composition and cell temperature on the positive electrode utilization of small-scale LiAl/FeS cells was prompted by the above out-of-cell experiments. The tests were conducted on LiAl (10 A-hr)/FeS (6.5 A-hr) cells with LiCl-KCl electrolytes having LiCl concentrations of either 53, 58 (eutectic), 63, or 67 mol % LiCl. All of these cells were operated at 450 and 500°C and at current densities of 50 and 100 mA/cm^2 (electrode area, 15.6 cm^2).

*Resident Associate from Institute of Nuclear Energy Research, Taiwan, Republic of China.

†Cell development and Engineering Group.

The test results, given in Table VI-2, show that the positive electrode utilization increases with increasing LiCl concentration and/or cell temperature. Satisfactory electrode utilization is achieved in cells using a lithium chloride concentration of 67 mol % and a cell temperature of 450°C. These results confirm the out-of-cell tests in the previous section.

Table VI-2. Utilization of Positive Electrode in LiAl/LiCl-KCl/FeS Cells

LiCl Concentration, mol %	Temp., °C	Current Density, mA/cm^2		FeS Electrode Utilization, %
		Charge	Discharge	
53	450	50	50	25
	500	50	50	44
	450	100	100	14
	500	100	100	40
58[a]	450	50	50	52
	500	50	50	70
	450	100	100	44
	500	100	100	55
63	450	50	50	74
	500	50	50	77
	450	100	100	68
	500	100	100	71
67	450	50	50	85
	500	50	50	90
	450	50	100	81
	500	50	100	85

[a]Eutectic composition.

VII. ADVANCED BATTERY RESEARCH
(M. F. Roche)

The objective of this work is to develop secondary cells that use inexpensive, abundant materials. The experimental work ranges from cyclic voltammetry studies and preliminary cell tests through the construction and operation of engineering-scale cells for the most promising systems. The studies at present are focussed on the development of calcium/metal sulfide cells having a materials cost of $10-15/kW-hr (in mass production) and a performance equivalent to the Mark III goals. The Mark III performance goals are as follows: specific energy, 160 W-hr/kg; energy density, 525 W-hr/L; peak specific power, 200 W/kg; and cycle life, 1000 cycles.

A. Engineering-Scale Cell Tests
(L. E. Ross, P. F. Eshman,* M. F. Roche)

A sealed, prismatic (13.5 × 13.5 × 2.5 cm) $Ca(Mg_2Si)/NiS_2$ cell with a theoretical capacity of 70 A-hr was put into operation during the last quarter (ANL-78-21, p. 63). This was fabricated in the uncharged state; the negative electrodes contained Mg_2Si powder, and the positive electrode contained calcium sulfide, Ni_3S_2,† and carbon fibers. The electrolyte was LiCl (54 mol %)-KCl (39 mol %)-$CaCl_2$ (7 mol %), and the cell operating temperature was 450°C.

Operation of this cell was terminated after 120 cycles due to declining coulombic efficiency. The cell performance for the 120 cycles is given in Fig. VII-1. Near cycle 65, the cell was cooled to room temperature, and additional $CaCl_2$ was added to raise the $CaCl_2$ concentration to 9.1 mol %. The intent was to determine the effect of a higher $CaCl_2$ concentration on specific energy, but this procedure led to a decline in coulombic efficiency. Beyond cycle 90, the charge cutoff voltage was decreased from 2.4 V to 2.3 V (the discharge cutoff voltage was 1.0 V), thereby resulting in a decrease of specific energy from ∿35 to ∿31 W-hr/kg at the 6-hr rate. The relatively low specific energy of this cell (∿42 W-hr/kg in early cycles) was partially due to two factors: the electrode materials were only 20% of the cell weight and the electrode and electrolyte compositions were not optimized for specific energy. Tests on large-scale cells with a design that is more compact than that of the above cell will be done after optimization studies of the active materials and electrolyte (discussed below) are completed.

---

*Industrial Cell and Battery Testing Group.

†Formed in the electrode from a mixture of Ni and NiS.

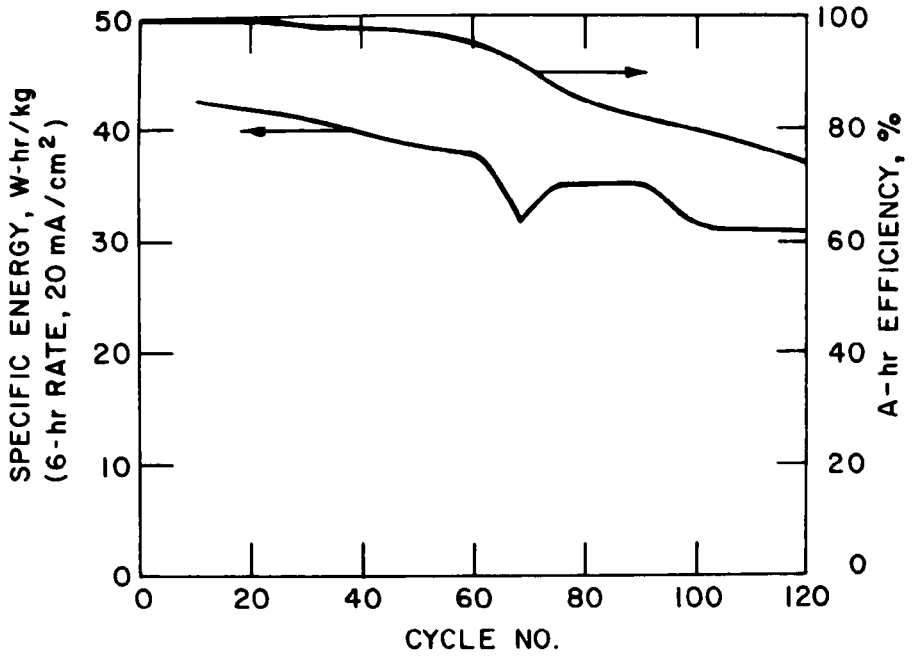

Fig. VII-1. Performance of $Ca(Mg_2Si)/NiS_2$ Cell.

B. Cell Development

1. Positive Electrode Development
(S. K. Preto)

Cyclic voltammetry experiments are being done to identify electrode and electrolyte compositions that lead to a high positive-electrode utilization in calcium/metal disulfide cells. In earlier studies (ANL-77-75, p. 51; ANL-78-21, p. 53) cyclic voltammetry experiments had been done on the FeS_2 and NiS_2 electrodes of lithium/metal disulfide cells; the voltammetry cell contained a NiS_2 or an FeS_2 working electrode, Li-Al reference and counter electrodes, and LiCl-KCl electrolyte. Lithium-ion reactions (*e.g.*, $2Li^+ + NiS_2 + 2e^- \rightarrow Li_2S + NiS$) were dominant in these earlier experiments. In this study, the voltammetry cell also contained a NiS_2 or an FeS_2 working electrode (~100 mg of the metal disulfide in carbon foam within a 5-cm^2 molybdenum housing). However, the reference and counter electrodes were $CaAl_4$, and the electrolyte was LiCl (54 mol %)-KCl (39 mol %)-$CaCl_2$ (7 mol %). The cell was operated at 430°C, and the working electrodes were cycled repeatedly over the range 1.0-2.0 V *vs.* $CaAl_4$ at a voltage scan rate of 0.02 mV/sec. Because CaS (ΔG_f° = -110 kcal/mol) is more stable than Li_2S (ΔG_f° = -100 kcal/mol), calcium-ion reactions (*e.g.*, $Ca^{++} + NiS_2 + 2e^- \rightarrow CaS + NiS$) were dominant in the present experiments.

With the NiS_2 electrode, four calcium-ion reactions were observed at approximately 1.79 V, 1.64 V, 1.59 V, and 1.43 V *vs.* $CaAl_4$, and were assigned to the reactions: $NiS_2 \leftrightarrow NiS$, $NiS \leftrightarrow Ni_7S_6$, $Ni_7S_6 \leftrightarrow Ni_3S_2$, and $Ni_3S_2 \leftrightarrow Ni$, respectively. Identical nickel-sulfide phases were assigned to the four lithium-ion reactions observed in the earlier voltammogram (ANL-77-75, p. 3), but the behavior of the reaction peaks in the two voltammograms differed in two respects. First, the separation between charge and discharge voltages

was 30-60 mV for the calcium-ion reactions, but was only 0-20 mV for the lithium-ion reactions. Thus, the calcium-ion reactions were somewhat less reversible than the lithium-ion reactions. Second, with the LiCl-KCl-$CaCl_2$ electrolyte, all four reactions exhibited a high initial capacity (more than 80% of theoretical), but only the reaction at the highest voltage, $NiS_2 \rightarrow NiS$ (1.79 V), exhibited good capacity retention during extended cycling (~20 cycles). The diminishing capacity of the lower voltage peaks (between 1.64 and 1.43 V) with cycling suggests some type of passivation mechanism. With the LiCl-KCl electrolyte, all four reactions also exhibited a high initial capacity, but unlike the case with LiCl-KCl-$CaCl_2$ only the lower-voltage reactions *i.e.*, ($NiS \rightarrow Ni_7S_6$, $Ni_7S_6 \rightarrow Ni_3S_2$, $Ni_3S_2 \rightarrow Ni$) exhibited good capacity retention during extended cycling. In this case, the diminishing capacity of the high-voltage peak with cycling suggests some type of mechanism for sulfur loss.

With the FeS_2 electrode, two major calcium-ion reactions were observed at approximately 1.78 V and 1.40 V *vs.* $CaAl_4$, and were assigned to the reactions $FeS_2 \leftrightarrow FeS$ and $FeS \leftrightarrow Fe$, respectively. In an earlier study of lithium-ion reactions (ANL-78-21, p. 53), the corresponding major reactions were $FeS_2 \rightarrow Li_3Fe_2S_4$ and $Li_2FeS_2 \rightarrow Fe$. With the LiCl-KCl-$CaCl_2$ electrolyte, only the reaction $FeS_2 \rightarrow FeS$ exhibited good capacity retention during extended cycling, whereas with the LiCl-KCl electrolyte only the reaction $Li_2FeS_2 \rightarrow Fe$ exhibited good capacity retention. This behavior is similar to that of the nickel-sulfide reactions in the two electrolytes. Again, differences in passivation and rates of sulfur loss may account for the differences in the capacity retention of the FeS_2 reactions with the two types of electrolytes.

The above study has indicated the need for a much more detailed examination of the effects of electrolyte on the metal-disulfide reactions. Cyclic voltammetry experiments will be conducted using alternative electrolytes such as LiCl-NaCl-$CaCl_2$-$BaCl_2$.

2. Negative Electrode Development
(L. E. Ross, M. F. Roche)

The Ca-Mg-Si ternary compounds presently used in calcium/metal sulfide cells are formed by charging Mg_2Si in a molten-salt electrolyte that contains calcium ions. The exact Ca-Mg-Si phases that form under these conditions are unknown, but they contain about 1 A-hr of calcium per gram of Mg_2Si, which corresponds to the empirical composition $Ca_{1.5}Mg_2Si$. Previous studies (ANL-77-35, p. 53) showed that the performance of the calcium electrode approaches that of the LiAl electrode. However, the Ca-Mg-Si alloy has two properties that might cause short circuits during long-term cycling. These properties are:

(1) If the cell is discharged to low potentials, the magnesium in Mg_2Si may form magnesium ions and subsequently may deposit as magnesium metal in the cell separator.
(2) During cycling, Mg_2Si forms 2-μm-dia particles which may escape from the negative electrode.

Therefore, we initiated a search for alternative alloys for use in the negative electrode. During this quarter, the utilization of Ca-Al-Zn and Ca-Pb

electrodes was determined in LiCl-KCl (eutectic composition) plus 7-9 mol % $CaCl_2$. In order to test the Ca-Al-Zn electrode, two small cells were cycled at 430°C. The first cell had a negative electrode of $CaAl_2$ (area, 15 cm^2; theoretical capacity, 6 A-hr) and a positive electrode of Al (area, 5 cm^2; theoretical capacity, ∿2 A-hr), and the second cell had the same negative electrode as the first but a positive electrode of Al-Zn (area, 5 cm^2; theoretical capacity, ∿2 A-hr). The utilization of both 2 A-hr electrodes was only 30% at a current density of 20 mA/cm^2. Thus, zinc additive did not improve the utilization of the Al electrode. Earlier tests of $CaAl_2$ electrodes (ANL-77-35, p. 53) indicated a maximum utilization of approximately 60% of their theoretical capacity (1.0 A-hr/g Al) at 485°C. The better utilization of the $CaAl_2$ electrode at a higher temperature suggests a reaction that is limited by solid-phase diffusion. Other additives will be tested in an effort to overcome these limitations.

A Ca-Pb electrode, which had a theoretical capacity of 0.78 A-hr/g $CaPb_3$ (assuming the electrode is cycled between Ca_3Pb and $CaPb_3$), was tested in the same manner as the Ca-Al-Zn electrode. The utilization of this cell was found to be 60% at a current density of 36 mA/cm^2. This electrode does not appear to be satisfactory for use in high-energy-density cells because of its relatively low theoretical capacity, but it may be useful for stationary energy storage applications. Future experiments will concentrate on tests of electrodes with high theoretical capacity, such as Ca_2Si (3.82 A-hr/g Si).

3. Electrolyte Development
(L. E. Ross, C. C. Sy, S. K. Preto)

The electrolyte now used in calcium/metal sulfide cells, LiCl (54 mol %)-KCl (39 mol %)-$CaCl_2$ (7 mol %), has a low melting point (∿350°C), but it is relatively expensive because of its high concentration of LiCl. Therefore, alternative electrolytes are under investigation. The following four chloride salts are inexpensive and compatible with the cell electrodes: $CaCl_2$, $BaCl_2$, NaCl, and KCl. Previous studies[9] determined the melting points of the following three electrolytes (composition in mol %), all of which contain these chloride salts: 33 NaCl-8 KCl-45 $CaCl_2$-14 $BaCl_2$, 29 LiCl-20 NaCl-35 $CaCl_2$-16 $BaCl_2$, and 38.5 NaCl-47 $CaCl_2$-14.5 $BaCl_2$. In preliminary experiments, the melting points of these three electrolytes were redetermined by measuring the temperature of solidification as the molten electrolyte was cooled. The previously reported melting points and the melting points determined in this study are listed in Table VII-1. The electrolyte with the lowest melting point

Table VII-1. Melting Points of Electrolytes

Electrolyte Composition, mol %					Melting Point, °C	
LiCl	NaCl	KCl	$CaCl_2$	$BaCl_2$	Reported[1]	This Study
-	33	8	45	14	421	453
29	20	-	35	16	378	390
-	38.5	-	47	14.5	450	440

was LiCl-NaCl-$CaCl_2$-$BaCl_2$ (mp 390°C); this electrolyte is now being tested in cyclic voltammetry studies and in small-cell tests to determine its effect on cell performance. In future studies, attempts will be made to lower the LiCl concentration of the electrolyte to ∿10 mol %.

REFERENCES

1. W. L. Towle, *et al.*, *Cost Estimate for the Commercial Manufacture of the Lithium/Iron Sulfide Cells for Load-Leveling*, Argonne National Laboratory Report, ANL-76-12, March 1976.

2. Private communication from Sandia Absalon, U. S. Bureau of Mines (March 1978).

3. Private communication from G. Griggs, U. S. Borax (March 1978).

4. Energy Research and Development Administration (ERDA), Office of Electric and Hybrid Vehicles, *Test and Evaluation Procedures for Electric Vehicles* (1976).

5. P. E. Evans, *Continuous Hot Compaction of Metal Powders*, Powder Metallurgy Metallurgy, Interscience Publisher, New York, p. 553 (1960).

6. C. R. Shakespeare and D. A. Oliver, *Mode Development in Powder Metallurgy*, Plenum Publ. Corp., New York, p. 253 (1966).

7. J. van Brakel, *Pore Space Models for Transport Phenomena in Pourous Media; Review and Evaluation with Special Emphasis on Capillary Liquid Technology*, Powder Tech, *11*, 205 (1975).

8. M. L. Saboungi, J. J. Marr, and M. Blander, *Solubility Products of Metal Sulfides in Molten Salts: Measurements and Calculations for Iron Sulfide (FeS) in the LiCl-KCl Eutectic Composition*, submitted for publication to J. Electrochem. Soc.

9. G. J. Janz, *et al.*, ERDA Publication No. TID-27163 (July 1976).

APPENDIX A.

Summary of Large-Scale Cell Tests January-March 1978

APPENDIX A. Summary of Large-Scale Cell Tests January-March 1978

Cell Description[a]	Max. Performance @ Indicated Rate[b] A-hr	W-hr	Rates, hr Disch.	Charge	Initial Eff.,[c] % A-hr	W-hr	Life Characteristics Days[d]	Cycles[d]	% Decline in[e] Capacity	Energy	A-hr Eff.	W-hr Eff.	Remarks
1A5, Li-Al/FeS-Cu_2S, C, 78/78, 13.5 × 15.6 × 2.3 cm, 1.35 kg	51.7 49.4 48.4	64.9 59.0 55.2	10 4 2.5	10 4 2.5	99	90	19	43	15	18	45	36	EP thin-electrode cell. Restarted to test LiCl-rich electrolyte. Decline in coulombic efficiency after 30 cycles. Terminated.
1B4, Li-Al/FeS-Cu_2S, C, 146/149, 13.5 × 15.6 × 3.8 cm, 2.0 kg	84	93	10	10	86	65 85	>707	>1223	29	25	30	26	EP thick-electrode cell. Previously in series with IB6. 1283 total cycles. Tested at 500°C (121 cycles). Now at 425°C.
I-3-B-1, Li-Al/FeS-Cu_2S, C, 170/127, 13.5 × 15.6 × 3.8 cm, 2.035 kg	101 88 76 68	131 108 92 73	10 5.9 3.8 2.7	10 5.9 3.8 2.7	99	81	>426	>686	6	9	3	3	EP cell, with slightly thinner positive and slightly denser negative than baseline Type 2B electrodes. 67 W-hr/kg at 10-hr rate.
I-3-B-2, Li-Al/FeS-Cu_2S, C, 170/127, 13.5 × 15.6 × 3.8 cm, 2.07 kg	85 77	104 88	8.5 5	8.5 5	99	82	>189	>305	4	4	2	9	Previously terminated after qualification tested (42 days, 48 cycles). Restarted to study cell operation at 500°C. Now operating at 425°C.
I-3-C-1, Li-Al/FeS-Cu_2S, C, 193/145, 13.5 × 15.6 × 3.8 cm (shimmed cell), 1.72 kg	62	76	6	6	99	84	>69	>70	0	0	8 0	9 0	Cell previously tested for 52 days, 51 cycles. Restarted to study open-circuit voltage as function of discharge state at 450°C and 500°C.
I-3-C-2, Li-Al/FeS-Cu_2S, C, 193/145, 13.5 × 15.6 × 3.8 cm (shimmed cell), 1.79 kg	97	112	10	10	98	84	292	527	57	49	46	48	EP cell, constant current compared to constant voltage charge. Tested at up to 525°C. Terminated due to poor performance.
I-8-B-5, Li-Al/FeS_2-CoS_2, C, 200/156, 13.5 × 15.6 × 3.8 cm (shimmed cell) 1.66 kg	110	152	11	11	93	77	46	53	56	60	74	78	EP cell built to study BN felt separator. Terminated, poor coulombic efficiency.

APPENDIX A. Summary of Large-Scale Cell Tests January-March 1978

Cell Description[a]	Max. Performance @ Indicated Rate[b] A-hr	W-hr	Rates, hr Disch.	Charge	Initial Eff.,[c] % A-hr	W-hr	Life Characteristics Days[d]	Cycles[d]	% Decline in[e] Capacity	Energy	A-hr Eff.	W-hr Eff.	Remarks
I-8-C-10, Li-Al/FeS_2-CoS_2, C, 200/156, 13.5 × 15.6 × 3.2 cm, 1.63 kg	99	137	20	20	78	69	23	18	0	0	50	50	EP cell built to test BN felt. Poor efficiency on initial cycles. Terminated.
I-8-E-16, Li-Al/FeS_2-CoS_2, C, 106/156, 13.5 × 15.6 × 3.8 cm, (shimmed cell) 1.9 kg	101 80	148 109	20 8	20 8	99	84	25	22	4	4	58	62	EP cell with Catalyst Research cast negative. Terminated, poor coulombic efficiency.
I-8-G-20, Li-Al/FeS_2-CoS_2, C, 75/150, 13.5 × 15.6 × 3.6 cm, 1.87 kg	40	61	4	4	97.5	78	61	129	0	5.1	0	14	Cycling restricted to 25% of FeS_2 capacity to check lifetime effects. Cell on standby, cycler needed for other test.
I-8-H-027, Li-Al/FeS_2-CoS_2, C, 148/117, 13.5 × 14.8 × 2.2 cm, 1.23 kg	76.0	109.0	7	8	98	80	33	48	21	23	18	16	EP cell. A similar cell examined at EP showed particle loss from the electrodes during electrolyte filling. Terminated, low coulombic efficiency.
I-8-H-041, Li-Al/FeS_2-CoS_2, S, 148/117, 13.5 × 15.6 × 2.3 cm, 1.22 kg	101	150	10	10	99	86	>13	>15	0	0	0	0	EP Type I-8 cell with Y_2O_3-felt retainers added to both electrodes. Initial cycles prior to qualification test.
I-8-K-032, Li-Al/FeS_2-CoS_2, C, 289/220, 13.5 × 15.6 × 3.8 cm, 1.87 kg	0	0	0	0	0	0	0	0	0	0	0	0	EP cell. A similar cell examined at EP showed particle loss from electrodes during electrolyte filling. Low frozen resistance. Cell short-circuited on first cycle.
I-8-K-033, Li-Al/FeS_2-CoS_2, C, 289/220, 13.5 × 15.6 × 3.8 cm, 1.87 kg	0	0	0	0	0	0	0	0	0	0	0	0	EP cell. A similar cell examined at EP showed particle loss from electrodes during electrolyte filling. Low frozen resistance. Cell short-circuited on first cycle.

APPENDIX A. Summary of Large-Scale Cell Tests January-March 1978

Cell Description[a]	Max. Performance @ Indicated Rate[b] A-hr	W-hr	Rates, hr Disch.	Charge	Initial Eff.,[c] % A-hr	W-hr	Life Characteristics Days[d]	Cycles[d]	% Decline in[e] Capacity	Energy	A-hr Eff.	W-hr Eff.	Remarks
I-8-L-034, Li-Al/FeS_2-CoS_2, C, 289/220, 13.5 × 15.6 × 3.8 cm, 1.71 kg	151	214	12	12	83	62	31	18	35	38	40	36	EP cell. One of cells subject to particle loss during salt filling. Cell qualification tested. 90 W-hr/kg at 4-hr rate. Decline in capacity. Terminated.
G-03-002, Li-Al/FeS-Cu_2S, U, 233/168, 14 × 21 × 3.6 cm, 2.73 kg	78	92	4	8	>98	81	>22	>45	14	14	10	10	Gould's first FeS baseline cell; Ca addition to negative. 44 W-hr/kg at 4-hr rate. Restarted for lifetime testing.
G-04-002, Li-Al/FeS_2-CoS_2, U, 139, 14.02 × 21.0 × 3.6 cm, 2.45 kg	116	191	10	10	98	86	20	25	2	4	1	2	Gould upper-plateau cell. Qualification tested. Cell on standby.
G-04-003A, Li-Al/FeS_2-CoS_2, U, 96, 14.02 × 21.0 × 3.6 cm, 2.02 kg	81 81	128 112	5.5 1.8	5.5 5.5	98	82	12	24	1	1	0	0	Gould upper-plateau cell. Cell short-circuited at end of qualification test.
G-04-005, Li-Al/FeS_2-CoS_2, 96, 14.02 × 21.0 × 3.8 cm, 2.05 kg	69	114	7	7	92	80	17	39	3	3	6	5	Gould upper-plateau cell, loss of efficiency near end of qualification test. Cell terminated.
G-04-006, Li-Al/FeS_2-CoS_2, U, 140/14.02 × 21.0 × 3.8 cm, 2.33 kg	113	186	10	10	99	86	>3	>3	0	0	0	0	Gould upper-plateau cell. Will undergo qualification testing.
G-04-009A, Li-Al/FeS_2, U, 180, 14.02 × 21.0 × 3.6 cm, 2.83 kg	162	252	11	11	96	80	21	23	0	0	0	0	Gould upper-plateau cell. Matrix testing completed, cell on standby.
G-04-010, Li-Al/FeS_2, CoS_2, U, 180, 14.02 × 21.0 × 3.8 cm, 2.77 kg	161	254	16	16	100	86	17	17	0	0	0	0	Gould upper-plateau cell. Testing completed. Cell on standby.
G-04-011A, Li-Al/FeS_2-CoS_2, U, 96.1, 14.02 × 21.0 × 3.8 cm, 2.18 kg	82	127	5.5	6	89	73	19	33	18	13	18	8	Gould upper-plateau cell. Terminated, poor efficiency.

APPENDIX A. Summary of Large-Scale Cell Tests January-March 1978

Cell Description[a]	Max. Performance @ Indicated Rate[b]		Rates, hr		Initial Eff., [c] %		Life Characteristics						Remarks
									% Decline in[e]				
	A-hr	W-hr	Disch.	Charge	A-hr	W-hr	Days[d]	Cycles[d]	Capacity	Energy	A-hr Eff.	W-hr Eff.	
G-04-012, Li-Al/FeS_2-CoS_2, U, 139, 14.02 × 21.0 × 3.6 cm, 2.5 kg	100	160	10	10	99	82	19	26	0	0	0	0	Gould upper-plateau cell. Terminated after matrix qualification test to make room for next cell.
G-04-013, Li-Al/FeS_2-CoS_2, U, 180, 14.02 × 21.0 × 3.6 cm, 2.85 kg	107	153	5.5	11	97	74	>45	>51	10	11	4	5	Gould upper-plateau cell. Very stable performance. Previously tested for 55 days and 68 cycles.
G-04-014, Li-Al/FeS_2-CoS_2, U, 155, 14.02 × 21.0 × 3.8 cm, 2.55 kg	125	188	8	8	99	80	14	19	0	0	0	0	Gould upper-plateau cell. Testing completed. Cell on standby.
G-04-014B, Li-Al/FeS_2-CoS_2, U, 146, 14.02 × 21.0 × 3.8 cm, 2.5 kg	111 108	180 158	10 7	10 7	96	83	13	18	0	0	0	0	Gould upper-plateau cell. Short-circuited.
G-04-015, Li-Al/FeS_2-CoS_2, U, 140, 14.02 × 21.0 × 3.8 cm, 2.44 kg	112	180	10	10	99	86	>14	>15	0	0	0	0	Gould upper-plateau cell. Will undergo qualification testing.
G-04-017, Li-Al/FeS_2-CoS_2, U, 96, 14.02 × 21.0 × 3.8 cm, 2.12 kg	86 85	132 108	6 1.5	6 6	99	83	15	27	0	0	0	0	Gould upper-plateau cell. Qualification testing finished. Cell on standby.
G-04-019A, Li-Al/FeS_2-CoS_2, U, 180, 14.02 × 21.0 × 3.8 cm, 2.8 kg	129	197	8.5	8.5	70	56	18	17	0	0	0	0	Gould upper-plateau cell. Poor efficiency initially. Cell shorted.
G-04-021A, Li-Al/FeS_2-CoS_2, U, 168, 14.02 × 21.0 × 3.6 cm, 2.84 kg	91	101	6	6	100	72	6	5	0	0	0	0	Gould FeS_2 upper-plateau cell. Terminated, unstable resistance.
G-04-022, Li-Al/FeS_2, U, 150, 14.02 × 21.0 × 3.6 cm, 2.83 kg	130	195	12	12	>99	76	18	20	0	0	0	0	Gould upper-plateau cell. Qualification tested. Cell on standby.
G-04-023, Li-Al/FeS_2-CoS_2, U, 100, 14.02 × 21.0 × 3.6 cm, 2.45 kg	77	112	5	5	98.5	72	10	20	0	0	0	0	Gould FeS_2 upper-plateau cell. Testing completed. Cell on standby.

APPENDIX A. Summary of Large-Scale Cell Tests January-March 1978

Cell Description[a]	Max. Performance @ Indicated Rate[b] A-hr	W-hr	Rates, hr Disch.	Charge	Initial Eff.,[c] % A-hr	W-hr	Life Characteristics Days[d]	Cycles[d]	% Decline in[e] Capacity	Energy	A-hr Eff.	W-hr Eff.	Remarks
G-04-025, Li-Al/FeS_2-CoS_2, U, 180, 14.02 × 21.0 × 3.8 cm, 2.83 kg	120	179	8	8	99	77	20	39	0	0	0	0	Gould FeS_2 upper-plateau cell. Matrix qualification testing completed. Cell on standby.
PMC-2-01, Li-Al/FeS_2-Mo, C, 156/164, 13.5 × 13.5 × 3.75 cm, 2.7 kg	85 61	108 73	5.5	8	95	70	50	92	10	10	14	11	Pellet cell. Test FeS_2-Mo electrode mix. Terminated, declining coulombic efficiency.
R-31, Li-Al/NiS_2-CoS_2, U, S, 159/132, 13.3 × 15.2 × 3.5 cm, 1.88 kg	83 65	108 79	8 3.5	8 6.5	100	81	>221	>513	20	28	10	14	Four-plateau NiS_2 cell, assembled semicharged with hot-pressed NiS + Li_2S positive. Negative electrode pressed Al wire, partially charged with Li foil.
R-32, Li-Al/NiS_2, U, 165/127, 13.3 × 15.2 × 3.5 cm, 1.90 kg	85 65	124 79	8 3.5	8 6.5	100	80	95	178	32	31	60	57	Four-plateau NiS_2 cell, assembled semicharged with hot-pressed NiS + Li_2S positive. Negative electrode pressed Al wire, partially charged with Li foil. Terminated.
R-34, Li-Al/FeS-Cu_2S, U, 151/115, 13.3 × 15.2 × 3.5 cm, 2.0 kg	85	101	4	11	98	78	88	144	11	9	15	15	Uncharged FeS cell with Cu additive. Positive contains high-temperature carbon. Negative electrode pressed Al wire, partially charged with Li foil. Cold-pressed positive. Terminated.
R-35, Li-Al/FeS_x-NiS_x-CoS_x, U, 144/120, 13.3 × 15.2 × 3.5 cm, 2.2 kg	117	117	15	16	97	81	43	50	44	50	43	50	Similar to R-30, except carbon fiber added to positive. Terminated.
R-36, Li-Al/NiS_2-Co_2S, U, 180/150, 13.3 × 15.2 × 3.5 cm, 1.8 kg	101 80	146 106	13.5 4	13.5 10	99	79	>92	>142	13	17	2	5	Similar to R-31, except high-temperature carbon added to positive electrode.
R-37, Li-Al/FeS, U, 180/150, 13.3 × 15.2 × 3.5 cm, 1.8 kg	64	76	3	8.5	99	78	>68	>148	15	18	4	3	Baseline FeS cell containing no additives in positive electrode.

APPENDIX A. Summary of Large-Scale Cell Tests January-March 1978

Cell Description[a]	Max. Performance @ Indicated Rate[b] A-hr	W-hr	Rates, hr Disch.	Charge	Initial Eff.,[c] % A-hr	W-hr	Life Characteristics Days[d]	Cycles[d]	% Decline in[e] Capacity	Energy	A-hr Eff.	W-hr Eff.	Remarks
R-38, Li-Al/FeS, U, 160/125, 13.3 × 15.2 × 3.5 cm, 1.8 kg	83	103	4.5	12	96	82	>50	>72	13	14	20	19	Similar to R-37 except LiCl-rich electrolyte used.
R-39, Li-Al/FeS, U, 129/121, 13.3 × 15.2 × 3.3, 1.73 kg	76	45	8	10	95	84	21	23	18	17	0	0	Similar to R-37 except ZrO_2 powder was added to the positive electrode. Terminated.
M-4, Li-Al/FeS_2-NiS-Mo-Fe, C, 165/267, 13.3 × 13.3 × 3.3 cm, 1.8 kg	135 112	187 159	9 4	9 8	99	81	172	300	17	21	18	22	EP cold-pressed negative/ANL hot-pressed positive electrodes. Y_2O_3 felt separator/retainer. 2.8-3.6 mΩ cell resistance. 70 W-hr/kg at the 2-hr rate. Terminated.
M-6, LiAl/FeS + Cu_2S, U, 158/128, 13.9 × 13.6 × 1.1 cm, 1.8 kg	111 75 68	135 81 78	11 4 2	15 11 8	100	82	44	64	16	4.5	0	0	Hot-pressed electrodes, 55 at. % LiAl in negative electrode. Pre-wet BN felt separator/retainer. Welded positive terminal. 3.9-4.9 mΩ cell resistance. Terminated.
M-7, Li-Al/FeS_2-NiS-Mo-Fe, C, 233/194, 13.3 × 13.5 × 2.7, 1.6 kg	118 102 80	173 149 116	8 4 1.6	9 9 8	96	84	>55	>80	14	16	11	12	Hot-pressed electrodes. Y_2O_3 felt separator/retainer. 2.4 mΩ cell resistance. 78 W-hr/kg at 2-hr rate and 97 W-hr/kg at 4-hr rate.
M-8, Li-Al/FeS, C, 155/113, 13.3 × 13.5 × 2.8, 1.5 kg	83 72	101 85	8 3.5	8 7	97	84	>10	>15	0	0	0	0	Hot-pressed electrodes. BN felt separator/retainer and LiCl-rich electrolyte. 3.5 mΩ cell resistance. 56 W-hr/kg at the 3.5-hr rate.
PW-8, Li-Al/FeS, 1/2 C, 190/115, 13.65 × 13.02 × 4.9 cm, 2.0 kg	63 35	78 39.7	12.6 2.3	12.6 4.7	99	86	>171	>408	0	3	0	1	MgO powder separator, vibratory loaded. Screens and frames on positive and negative electrodes. Use of M-series cell design.

APPENDIX A. Summary of Large-Scale Cell Tests January-March 1978

Cell Description[a]	Max. Performance @ Indicated Rate[b] A-hr	W-hr	Rates, hr Disch.	Charge	Initial Eff.,[c] % A-hr	W-hr	Life Characteristics Days[d]	Cycles[d]	% Decline in[e] Capacity	Energy	A-hr Eff.	W-hr Eff.	Remarks
PW-9, Li-Al/FeS, 1/2 C, 216/144, 13.65 × 13.02 × 4.2 cm, 1.94 kg	12 69	114 82.6	18.4 6.9	18.4 9.3	99	82	>65	>130	10	14	0	5	MgO powder separator, vibratory loaded. Screens and frames on positive and negative electrodes. Use of M-series cell design.
PW-10, Li-Al/FeS, 1/2 C, 190/131, 5.63 × 13.97 × 2.8 cm, 1.6 kg	49.7	60.6	5	6.7	98.6	84.9	>63	>104	19	25	0	7	Vibratory loaded 2-mm-thick separator layer of MgO powder. M-series design. Frames and screens or negative and positive electrodes.
KK-13, Li-Al/NiS_2-CoS_2, C, 160/210, 13.3 × 13.6 × 3.6 cm, 1.7 kg	120 100	177 137	10 4	12 4	99+	80	>170	>310	16	16	30	30	Carbon-bonded Li_2S + Ni_2S + CoS_2 positive, and LiAl pressed + Al wire negative. Welded Mo current collector. Y_2O_3 felt separator. 78 W-hr/kg at 4-hr rate. Cell accidently overcharged.

[a] The letters U, C, O, and S are used to indicate uncharged, charged, open, and sealed cells, respectively. The capacity ratio is the number of ampere-hours in the negative electrode over the number of ampere-hours in the positive electrode. In some cases, only the capacity of the limiting electrode is given.

[b] Based on at least five cycles.

[c] Based on at least 10 cycles at the 5-hr dishcarge rate.

[d] The "greater than" symbols denote continuing operation.

[e] Percent decline from the maximum values at the 5-hr discharge, except where noted.

Distribution for ANL-78-45

Internal:

M. V. Nevitt
R. V. Laney
P. R. Fields
S. A. Davis
B. R. T. Frost
G. T. Garvey
D. C. Price
K. E. Anderson
J. D. Arntzen
J. Barghusen
D. L. Barney (50)
L. Bartholme
J. E. Battles
E. C. Berrill
C. A. Boquist
L. Burris
F. A. Cafasso
A. A. Chilenskas
K. Choi
P. Cunningham
D. Day
W. DeLuca
R. Dunne
R. Elliott
W. R. Frost
E. C. Gay
J. Harmon
F. Hornstra
A. A. Jonke
R. W. Kessie
G. M. Kesser
V. M. Kolba
W. Kremsner
M. L. Kyle
W. W. Lark
S. Lawroski
R. F. Malecha
A. E. Martin
F. J. Martino
C. A. Melendres
A. Melton
W. E. Miller
F. Mrazek
K. M. Myles
T. Olszanski
P. A. Nelson (50)
E. G. Pewitt
E. R. Proud
S. Preto
G. Redding
M. F. Roche
L. E. Ross
M. Saboungi
W. W. Schertz
J. L. Settle
H. Shimotake
J. A. Smaga
R. K. Steunenberg
B. Swaroop
C. A. Swoboda
Z. Tomczuk
R. Varma
D. R. Vissers
S. Vogler
W. J. Walsh
D. S. Webster
S. E. Wood
N. P. Yao
P. Eshman
J. E. A. Graae
J. L. Hamilton
P. A. Eident
T. D. Kaun
J. E. Kincinas
K. Kinoshita
Z. Nagy
K. A. Reed
M. A. Slawecki
N. Otto
C. Sy
R. B. Poeppel
B. Bandyopadhyay
A. B. Krisciunas
ANL Contract File
ANL Libraries (5)
TIS Files (6)

External:

DOE-TIC, for distribution per UC-94cb (353)
Chief, Office of Patent Counsel, CH
V. Hummel, DOE-CH
President, Argonne Universities Association
Chemical Engineering Division Review Committee:
- C. B. Alcock, U. Toronto
- R. C. Axtmann, Princeton Univ.
- R. E. Balzhiser, Electric Power Research Institute
- J. T. Banchero, Univ. Notre Dame
- T. Cole, Ford Motor Corp.
- P. W. Gilles, Univ. Kansas
- R. I. Newman, Allied Chemical Corp.
- G. M. Rosenblatt, Pennsylvania State Univ.

J. G. Ahlen, Illinois Legislative Council, Springfield
J. W. Alpha, Corning Glass Works
J. Ambrus, Naval Surface Weapons Center
J. N. Anand, Dow Chemical Co., Walnut Creek, Calif.
F. Anson, California Inst. Technology
P. Auh, Brookhaven National Laboratory

B. S. Baker, Energy Research Corp.
H. Balzan, Tennessee Valley Authority
K. F. Barber, Div. Transportation Energy Conservation, USDOE
H. J. Barger, Jr., U. S. Army MERDC, Fort Belvoir
R. W. Barnes, Lithium Corp. of America, Gantonia, N.C.
T. R. Beck, Electrochemical Technology Corp., Seattle
J. A. Belding, Div. Conservation Research & Technology, USDOE
M. Benedict, Massachusetts Institute of Technology
D. N. Bennion, Univ. California, Los Angeles
J. Birk, Electric Power Research Inst.
J. Braunstein, Oak Ridge National Laboratory
M. Breiter, GE Research & Development Center
J. O. Brittain, Northwestern U.
R. Brodd, Parma Technical Center, Union Carbide Corp.
J. J. Brogan, Div. Transportation Energy Conservation, USDOE
E. Brooman, Battelle Memorial Institute, Columbus
B. D. Brummet, McGraw-Edison Co., Bloomfield, NJ
D. M. Bush, Sandia Laboratories
E. Buzzelli, Westinghouse Electric Corp., Pittsburgh
E. J. Cairns, General Motors Research Lab., Warren, Mich.
E. Carr, Eagle-Picher Industries, Joplin
P. Carr, Energy Development Associates, Madison Heights, Mich.
Chloride Systems (U. S. A.) Inc., North Haven, Conn.
C. Christenson, Gould Inc.
C. A. Clemons, PPG Industries, Pittsburgh
M. Cohen, Univ. of Chicago
A. R. Cook, Int'l Lead Zinc Research Organization, Inc., New York City
D. R. Craig, Hooker Chemical Corp.
G. Cramer, Southern California Edison, Rosemead
F. M. Delnick, Sandia Labs.
H. Dietrich, Fiber Materials, Inc., Biddeford, Mass.
D. L. Douglas, Gould Inc., Rolling Meadows
E. Dowgiallo, MERADCOM, Ft. Belvoir
J. Dunning, General Motors Research Lab., Warren, Mich.
P. Eggers, Battelle Memorial Institute, Columbus
M. Eisenberg, Electrochimica Corp.
R. P. Epple, Div. Physical Research, USDOE
P. L. Fleischner, National Beryllia Corp.
J. H. B. George, Arthur D. Little, Inc.
J. Giner, Giner, Inc., Waltham, Mass.
G. Goodman, Globe-Union, Inc., Milwaukee
G. Gorten, Gorten and Associates, Sherman Oaks, Calif.
H. Grady, Foote Mineral Co., Exton, Pa.
S. Gratch, Birmingham, Mich.
D. Gregory, Institute of Gas Technology, Chicago
N. Gupta, Ford Motor Co.
N. Hackerman, Rice U.
G. Hagey, Div. of Technology Overview, USDOE
C. Halpin, Halpin Engrs. Grosse Point, Mich.
R. Hamilton, Carborundum Co., Niagara Falls
W. Hassenzahl, Los Alamos Scientific Laboratory
L. A. Heredy, Atomics International
B. Higgins, Eagle-Picher Industries, Joplin
R. Hudson, Eagle-Picher Industries, Joplin

J. R. Huff, U. S. Army Mobility Equipment R&D Center, Fort Belvoir
R. A. Huggins, Stanford U.
R. A. Huse, Public Service Electric & Gas Co., Newark, N.J.
S. D. James, U. S. Naval Surface Weapons Center
M. A. Jansen, Allegheny Power Service Corp., Greensburgh, Pa.
G. Janz, Rensselaer Polytechnic Inst.
H. Jensen, C&D Batteries, Plymouth Meeting, Pa.
F. Kalhammer, Electric Power Research Institute
M. Katz, Div. Energy Storage Systems, USDOE
K. Kinsman, Ford Motor Co.
R. Kirk, Div. of Transportation Energy Conservation, USDOE
K. W. Klunder, Div. of Energy Storage Systems, USDOE
J. Lagowski, Detroit Edison Utility Co.
J. J. Lander, Air Force Aero Propulsion Lab., Wright-Patterson AFB
A. Landgrebe, Div. of Energy Storage Systems, USDOE (6)
C. E. Larson, Bethesda, Md.
S. H. Law, Northeast Utilities, Hartford, Conn.
H. Leribaux, Texas A&M U.
D. Linden, U. S. Army Electronics Command, Fort Monmouth, N.J.
R. Llewellyn, Indiana State U.
P. S. Lykoudis, Purdue Univ.
G. Mamantov, U. Tennessee
J. Mathers, U. Maryland
C. J. Mazac, PPG Industries, Corpus Christi
J. McKeown, Office of Program Administration, USDOE
C. McMurty, Carborundum Co., Niagara Falls
R. McRae, ILC Technology, Sunnyvale, Calif.
D. Meighan, C&D Batteries, Plymouth Meeting, Pa.
R. C. Miller, Kawecki Berylco Industries, Inc., Boyertown, Pa.
R. Minck, Ford Motor Co.
F. Moore, Div. of Energy Storage Systems, USDOE
R. Murie, General Motors Corp., Warren, Mich.
G. Murray, Detroit Edison Utility Co.
J. Nowabilski, Union Carbide Co., Tonawanda
C. Pax, Div. Transportation Energy Conservation, USDOE
G. F. Pezdirtz, Div. of Energy Storage Systems, USDOE
R. K. Quinn, Sandia Labs.
R. Rightmire, Standard Oil of Ohio, Cleveland
P. F. Ritterman, TRW Inc., Redondo Beach
R. Rizzo, Globe-Union, Inc., Milwaukee
N. Rosenberg, Transportation Systems Center, Cambridge, Mass.
N. W. Rosenblatt, E. I. duPont de Nemours & Co., Wilmington
R. Rubischko, Gould Inc.
A. Salkind, ESB Inc., Yardley, Pa.
W. Schaefer, Commonwealth Edison, Maywood, Ill.
G. Scharbach, American Motors General Corp., Wayne, Mich.
T. Schneider, Public Service Electric & Gas Co., Newark, N.J.
R. I. Schoen, National Science Foundation
J. R. Schorr, Battelle Memorial Institute, Columbus
D. R. Schramm, Public Service Electric & Gas Co., Newark, N.J.
H. J. Schwartz, NASA Lewis Research Center
J. R. Selman, Illinois Institute of Technology
A. I. Snow, Atlantic Richfield Co., Harvey, Ill.
S. Srinivasan, Brookhaven National Laboratory

D. Stakem, Catalyst Research Corp., Baltimore
E. Steeve, Commonwealth Edison Co., Chicago
R. H. Strange II, National Science Foundation
R. L. Strombotne, U. S. Dept. Transportation, Washington
S. Sudar, Atomics International
R. H. Swoyer, Pennsylvania Power and Light Co., Allentown
F. Tepper, Catalyst Research Corp., Baltimore
L. Thaller, NASA Lewis Research Center
G. M. Thur, Div. Transportation Energy Conservation, USDOE
C. W. Tobias, U. California, Berkeley
L. Topper, National Science Foundation
W. Towle, Globe-Union, Inc., Milwaukee
A. A. Uchiyama, Jet Propulsion Lab.
J. Vanderryn, Office of Intern, R&D Programs, USDOE
J. V. Vinciguerra, Eagle-Picher Industries, Joplin
R. D. Walker, Jr., U. Florida
C. O. Wanvig, Jr., Globe-Union, Inc., Milwaukee
S. A. Weiner, Ford Motor Co.
J. Werth, ESB Inc., Yardley, Pa.
C. Wienlein, Globe-Union, Inc., Milwaukee
F. Will, General Electric R&D Center, Schenectady
J. Withrow, Chrysler Corp., Detroit
S. E. Wood, El Paso, Tex.
T. Wydeven, NASA Ames Research Center
O. Zimmerman, Portland General Electric Co., Portland, Ore.
M. Zlotnick, Div. Conservation Research and Technology, USDOE
Chloride Technical Limited, Manchester, England
L. Pearce, Admiralty Materials Lab., Holten Heath, England
E. Voss, Varta Batterie A.G., Kelkhern, Germany
E. Aiello, U. of Chicago
W. J. Argersinger, Jr., U. of Kansas
J. T. Banchero, U. of Notre Dame
K. J. Bell, Oklahoma State U.
R. Blanco, Oak Ridge Nat. Lab.
C. F. Bonilla, Columbia U.
W. Brandt, U. of Wisconsin-Milwaukee
A. E. Dukler, U. of Houston
W. J. Frea, Michigan Tech. U.
J. E. Linehan, Marquette U.
Maine Univ., Prof. in charge of Chem. Engr. Lib.
Marquette U., Dept. of Chemistry
Michigan Tech. U., Library
N. R. Miller, United Nuclear Industries, Richland
G. Murphy, Iowa State U.
E. A. Peretti, U. of Notre Dame
G. W. Preckshot, U. of Missouri
H. Rosson, U. of Kansas
C. Sanathanan, U. of Illinois-Chicago Circle
A. Sesonske, Purdue U.
USDOE, Director, Div. of Safeguards and Security
B. W. Wilkinson, Michigan State U.
Comision Nacional de Energia Atomica, Library, Argentina
J. A. Sabato, Com. Nac. de Energia Atomica, Buenos Aires, Argentina
C. H. Cheng, Nat'l Tsing Hau Univ., China

National Radiological Protection Board, Library, Harwell, England
L. Kemmerich, Ges. fur Kernforschung, Karlsruhe, Germany
F. Weigel, Inst. fur Anorganische Chemie der U. Munich, Germany
N. Saratchandran, Bhabha Atomic Research Centre, Bombay, India
K. Fujimiya, U. of Tokyo, Japan
Japan Atomic Energy Research Inst., Tokai-mura, Japan
K. Matsuda, Inst. of Physical & Chemical Res., Yamato-machi, Japan
Sang-Soo Lee, Korea Advanced Institute of Science, Korea
Korean Atomic Energy Research Institute, Korea
Ragnar Nordberg, Sahlgren's Hospital, Göteborg, Sweden